The Roles of Intrinsic Barriers and Crystal Fluidity
in Determining the Dynamics of Crystalline
Molecular Rotors and Molecular Machines

Morgan E. Howe, Miguel A. Garcia-Garibay*

Department of Chemistry and Biochemistry, University of California—Los Angeles, Los Angeles, California 90095-1569

Abstract: Crystalline solids are a promising platform for the development of molecular machines. They have the potential of combining the molecular-level control of physical properties caused by isomerizations, conformational motions, or chemical reactions with the emergent properties that arise from long-range order and multiscale phenomena. However, the construction of crystalline molecular machinery has been challenging due to the difficulties associated with the design of structures capable of supporting high order and controlled molecular motion in the solid state, a platform that we term amphidynamic crystals. With ultrafast rotation as the target, previous work on amphidynamic crystals has explored the creation of free space around the rotator, the advantages of volume-conserving rotational motions, and the challenges associated with correlated rotations, or gearing motions. In this perspective we report the results of a systematic analysis of a large number of examples from our work and that others, where we demonstrate that the creation of free space alone does not always result in ultrafast dynamics. In a limit that applies to porous crystals with large empty volumes such as MOFs and other

extended solids, internal motions fall in the regime of activation control, with dynamics determined by the intrinsic (gas phase) electronic barriers for rotation around the bond that connects the rotator and the stator. By contrast, internal rotation in close-packed molecular crystals falls in the regime of diffusion-controlled dynamics, and depends on the ability of the rotator surroundings to distort and create transient cavities. We refer to this property as "crystal fluidity" and suggest that it may be used as an additional guiding principle for the design of crystalline molecular machines. We describe here the general principles behind the promising field of crystalline molecular machinery, the analytical methods to analyze rotational dynamics of crystalline solids, and the key structural concepts that may help their future development.

1. Molecular Machinery

Early concepts in the field of artificial molecular machines were based on appealing structural or functional analogies between macroscopic machines and molecules in solution, including gears, propellers, shuttles, and brakes. This work relied on and promoted advances in the field of dynamic stereochemistry and helped the development of analytical tools to document the trajectories, equilibria, and kinetics of complex conformational motions.² Subsequent developments recognized that artificial molecular machinery would require structures that not only display the desired machine-like motion, but that can be controlled under the influence of selected inputs, leading to the development of bistable molecular switches that operate on the basis of binding interactions, pH, redox processes, light absorption, and other suitable stimuli.³ The design of structures based on the synchronized behavior of integrated components to perform sophisticated tasks led to the development of unidirectional motors, molecular pumps, 5 and artificial muscles⁶ by the groups of Bernard L. Feringa, J. Fraser Stoddart, and Jean-Pierre Sauvage, respectively, which was recognized with the 2016 Nobel Prize in Chemistry. Having developed the use of molecular dynamics and function to accomplish specific tasks in solution.⁷ workers in the field have embraced the challenge of taking molecular-level functions into largerscale systems, including surfaces, ⁸ silica nanoparticles, ⁹ gels¹⁰ and crystalline solids^{11,12} among others. 13

2. Crystalline Molecular Machines

Our group has been interested in the development of artificial molecular machinery under conditions of reduced entropy by taking advantage of crystalline solids.¹¹ We recognize not only that structural elements on a molecular scale determine supramolecular interactions that lead to crystallization, but also that the presence of functional groups and molecular-scale structural

features can be used to engineer reactivity and internal molecular dynamics in the crystalline state. 11 Crystalline molecular machines have the potential of combining the molecular-level control of physical properties caused by isomerizations, conformational motions, or chemical reactions with the emergent properties that arise from changes in long-range order, including macroscopic changes such as salient phenomena in the form of shape changes, crystal moving, or jumping. 14 Depending on the characteristics of their constituents, crystalline molecular machines will be well suited for the long-range directional propagation and transduction of mechanical, thermal, electrical, magnetic and optical stimuli. 15 These characteristics make it possible to consider the use of controlled molecular motions in crystals to modulate physical properties, such as color, emission of light, polarization, conductivity, magnetism and optics, to chemical properties, such as catalysis, molecular storage, and sieving. Furthermore, crystalline molecular machines will be an ideal platform to translate advanced molecular-level design and function to properties that are harvested at larger scales, covering dimensions from tens of nanometers and microns, to the macroscopic dimensions of a human operator.

As a starting point to explore this promising new area of science and technology, we have selected a target platform that consists of an ordered array of interacting dipoles¹⁶ mounted on molecular rotors.¹⁷ These dipoles are capable of undergoing rapid reorientation in response to internal and external electric and electromagnetic fields, in a manner that resembles a collection of macroscopic compasses.¹¹ As shown in Figure 1a, crystalline arrays of freely rotating molecular dipoles are expected to develop spontaneous ordering that depends on their symmetry.¹⁸ Strong homogeneous fields can be used to alter the orientation of the dipoles to develop macroscopic polarization or to change its direction. This is illustrated in Figure 1b by a hypothetical crystal spontaneously adopting a non-polar antiferroelectric state that can be forced

into alignment and macroscopic polarization by an external field. Alternatively, local perturbations are expected to result in the propagation of rotary waves across the crystal, which may provide new mechanisms for signal transport and transduction. Changes in physical properties resulting from different dipole configurations and dipolar motion can be interfaced with other stimuli (sound waves, heat transfer, color, light, polarization, charge, *etc.*) to provide a variety of emergent functions.¹⁵

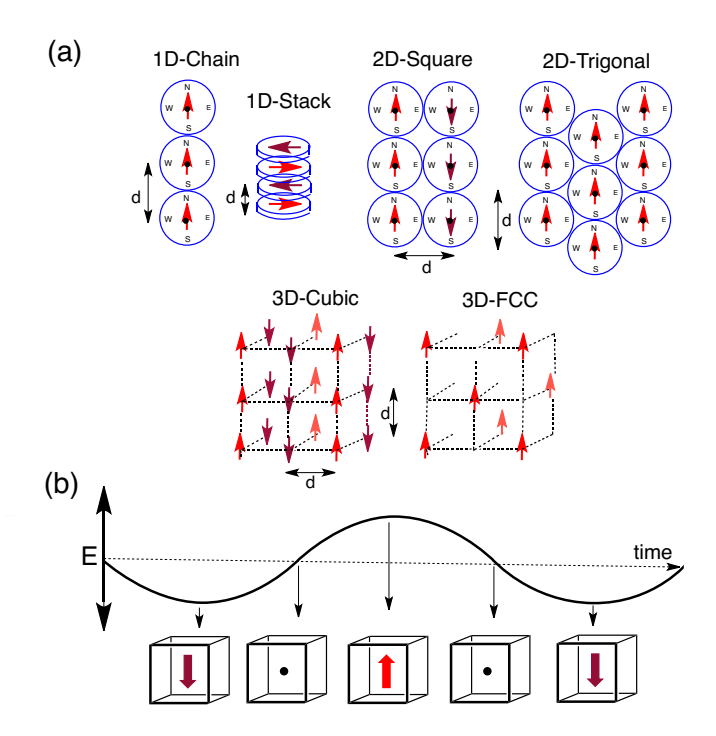


Figure 1. (a) Spontaneous order ideally expected from simple 1D, 2D, and 3D dipolar arrays with different symmetries. Some symmetries are expected to have an infinite number of degenerate ground state orientations, which would result in collectively coupled rotational states. (b) Expected macroscopic polarization of a hypothetic antiferroelectric 3D cubic crystal that has no spontaneous polarization (at E=0) but becomes macroscopically polarized in the presence of an external electric field (E≠0), whether the field is oscillating (as shown) or static.

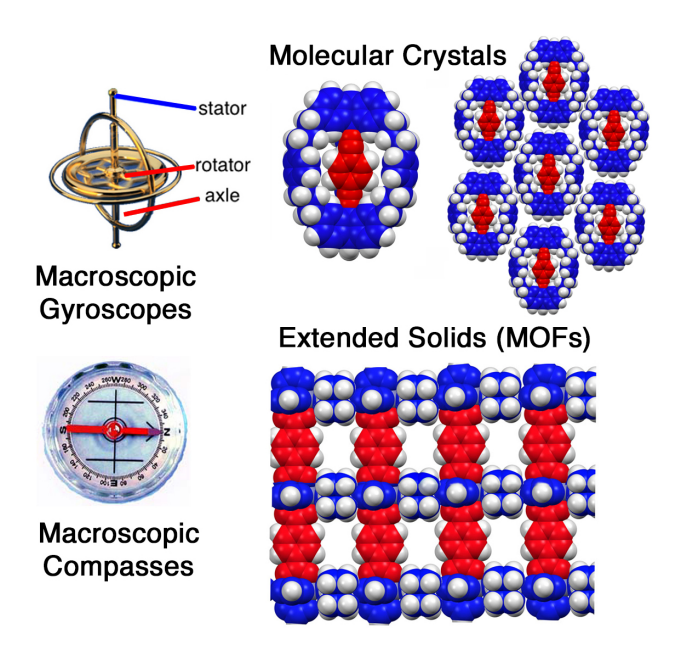


Figure 2. Structure of a macroscopic gyroscope illustrating its stator, rotator and axle, compared with the topologies and space-filling model of potential crystal-forming molecular rotors with closed and open topologies. The blue color is used to represent the stator and the red color is used to highlight the axle and the rotator.

3. Amphidynamic Crystals 11,19

The realization of crystalline rotary dipolar arrays requires molecular structures that can form an ordered lattice and support the rotation of the central dipole. To attain a strong alignment, dipole-dipole interactions should be large, their distances should be short, and the dielectric constant of the medium should be low to diminish the attenuation of their interaction. However, the most important requirement is to have their rotary motion unhindered. In fact, the design of crystalline molecular machines based on functions that rely on mechanical motions requires the construction of crystals with moving parts, which are also known as "amphidynamic crystals." For the original entry into the construction of amphidynamic crystals and dipolar arrays, we envisioned

structures analogous to those of macroscopic compasses and gyroscopes. As shown in Figure 2, these are formed by lattice-building, encasing structures (shown in blue) covalently connected by an axle to the rotating element (shown in red). Promising solutions for the construction of amphidynamic crystals can be based on extended solids with porous architectures, such as metalorganic frameworks (MOFs) where the functional rotators act as pillars linked by coordination bonds to static metal clusters. Also illustrated in Figure 2, more challenging solutions may be based on the use of close-packing interactions between discrete molecular units. These two types of materials will be the primary focus of this account.

4. Amphidynamic Crystalline Molecular Rotors Based on Free Volume, the Use of Axially Symmetric Rotators, and/or Correlated (Gearing) Motion Strategies

While exploring structural solutions for the construction of amphidynamic crystals based on molecular units, we envision molecules with structures that are similar to those of macroscopic gyroscopes. They may have closed topologies formed by bridging units that link the upper and lower portions of the stator, as shown in Figure 2, or open topologies where the bridges are absent and the enclosure is formed by the surrounding molecules in the lattice. When considering the structural elements that may allow for internal molecular rotation in a crystal, we proposed three solutions: (1) the creation of empty space, (2) an increase in the axial symmetry order of the rotator, and (3) the development of correlated motions. Empty space allows for unhindered motion, examples of which can be found in the extended networks of porous solids. Ultrafast hindered rotation, hindered rotation, and motion-gated diffusion have been documented using MOFs. High symmetry strategies assume the presence of short-range van der Waals interactions where adjacent molecules tend to conform to the shape of the rotator, such that the shape of its own cross section determines the height of the barriers it must overcome. Assuming smooth

polygonal (rather than ratcheted) structures, one can recognize that a rotator with a C_n rotational symmetry axis will have "n" degenerate energy minima connected by $360/n^o$ angular displacements. Furthermore, as $n \rightarrow \infty$ the shape of the rotator approaches the shape of a sphere or a cylinder, such that any steric hindrance begins to disappear. The third and most challenging approach is the design of correlated motions with high axial symmetry but inter-digitated structures where the rotation of one unit is geared with the rotations of one or more of its close neighbors.

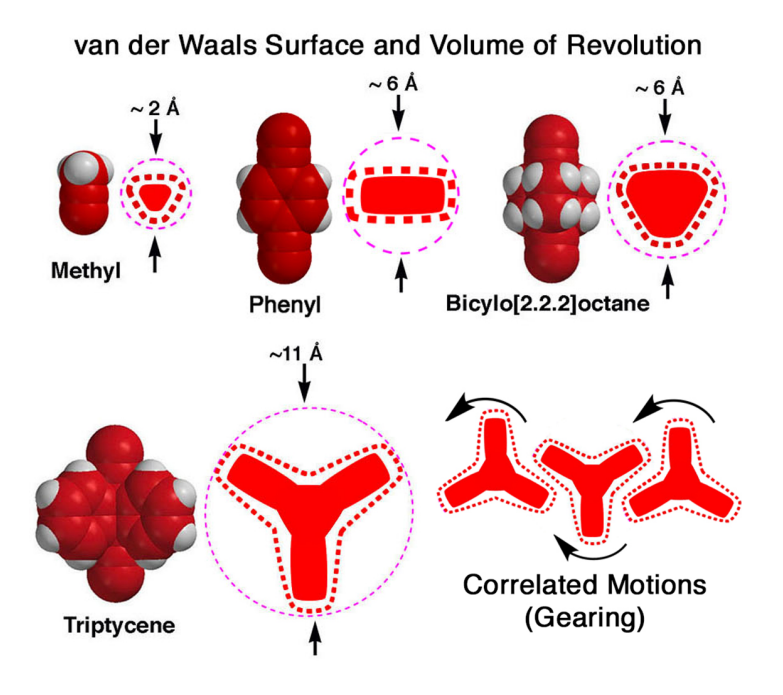


Figure 3. Space filling models of methyl, phenylene, and BCO rotators with a schematic cross section of their van der Waals surface (thick red lines) and their volume of revolution (thin magenta circles). Knowing that near neighbors tend to maximize surface contacts, one may expect that in the absence of free volume, the rotation of more spherical methyl and BCO rotators will be much less hindered than rotation of phenylene or triptycene rotators. In the absence of free volume, triptycene can only rotate by a correlated motion mechanism.

To visualize these limits in the context of closed packed molecular crystals, we need to consider the size and shape of the rotator, which may be represented by its van der Waals surface (Figure 3, thick dotted line) and the volume of revolution (thin dashed circle) that it creates as it rotates.²⁵ As illustrated in Figure 3 with hypothetical methyl, 1,4-phenylene, 1,4-bicyclo[2.2.2]octane (BCO), and 9,10-triptycene rotators, the van der Waals surface represents the closest approach that the rotator is likely to have with any static element in the lattice.

A three-fold symmetric methyl group is close to spherical, and its van der Waals volume is very close to its volume of revolution, with a small ca. 2 Å diameter. Similarly, BCO rotators have a fairly regular, three-fold symmetric van der Waals surface, and have a volume of revolution that approaches a cylinder with a diameter of ca. 6 Å. It should therefore not be surprising that methyl groups have nearly unhindered rotation in the solid state, ²⁶ and that BCO rotators have been shown to have relatively low solid-state barriers, generally in the range of ca. 1-4 kcal/mol.²⁷ By contrast, the cross section of a phenylene rotator reveals that its van der Waals surface approaches a rectangular shape, such that most close-packed crystals will fill a rectangular shaped space (thick dotted line) in order to have optimal packing interactions. Therefore, even though the volume of revolution of phenylene and BCO rotators have similar diameters (ca. 6Å), one may expect that phenylene rotation will generally be hindered, such that its use will require architectures with free volume or able to undergo correlated motions for rotation to take place. Finally, triptycene illustrates an example of a high-symmetry (three-fold) "star"-shaped rotator that requires either the design of structures with free volume extending beyond its van der Waals surface in order to accommodate its volume of revolution (ca. 11 Å) or a structure where close neighboring triptycenes rotate in a geared fashion, as illustrated in the bottom right portion of Figure 3.

The creation of free volume in close-packed molecular crystals is a significant challenge.

Using the potential energy diagram in Figure 4, we consider the energetic adversities that arise when one attempts to maintain two benzene molecules at a given distance.²⁸ We will refer to the same figure to explore some of the solutions.

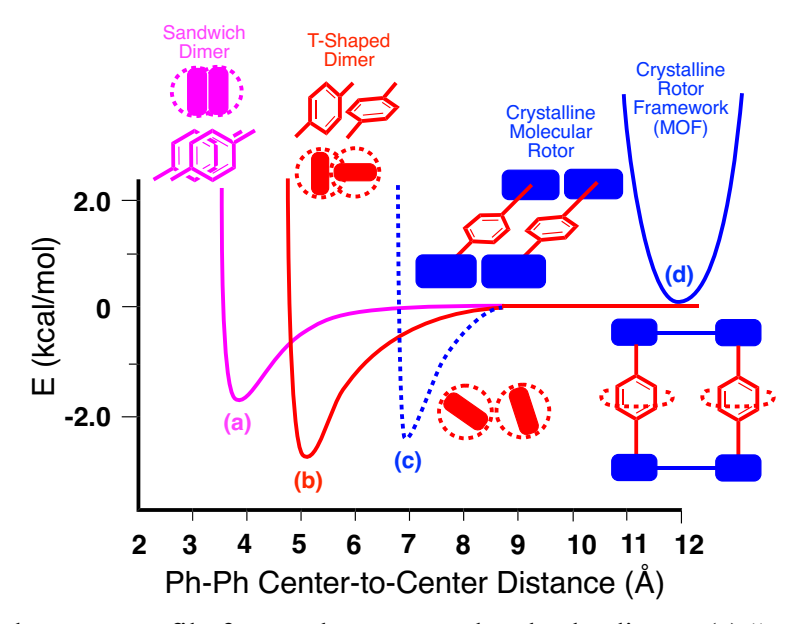


Figure 4. Potential energy profile for two benzene molecules leading to (a) "sandwich" and (b) "T-shaped" dimer structures, and as part of crystal structures based on (c) molecular crystals and (d) metal organic frameworks.

The magenta line (a) in Figure 4 represents the potential energy for two benzene molecules coming to their closest approach to form a sandwich dimer with a center-to-center distance of *ca*. 3.7-3.8 Å.²⁸ One can see how the two molecules fill in a significant fraction of each other's volume of revolution, making it impossible for them to rotate (a parallel-displaced dimer is actually more stable, but is less relevant to our analysis and is not included in the Figure). The red line (b) illustrates the energy changes as two benzene molecules approach each other in a T-shaped configuration with a center-to-center distance of *ca*. 4.9-5.0 Å.²⁸ Their overlapping volumes of revolution suggest that while they should be able to rotate, it would have to be in a

correlated manner. One can hypothesize that for two parallel benzene molecules to rotate independently, they would have to be at a center-to-center distance of ca. \geq 7.0 Å. In molecular crystals, this separation would require a stable framework created by a suitable stator, as suggested by the blue blocks. Close-packing interactions in this case would have to be satisfied by sufficient contact between adjacent stators, with their energy represented by the dotted blue line. However, the free volume generated in this case may have a tendency to trap solvent molecules or lead to the collapse of the crystal lattice. The final scenario is illustrated by benzene molecules at distances greater than ca. 9Å, which make it possible for the molecules to rotate independently. Notably, large free volumes can remain stable in solid-state systems that are well beyond the attractive region of the intermolecular potential and also take advantage of coordination and covalent bonds to create robust structures. These structures give rise to the solid blue potential, examples of which can be found in a number of MOFs. 29

5. Rotational Dynamics and Packing Coefficients

A measure of the average free volume that exists in a crystalline solid can be obtained by determination of the packing coefficient (C_k) , 30 which is given by the volume of the unit cell contents (V_{Mol}) in relation to the volume of the unit cell (V_{Cell}) , $C_k = V_{Mol} / V_{Cell}$. It can be expected that packing forces will tend to make the maximum number of surface contacts, which will depend on the shape of the molecule. For example, it has been shown that the densest 3D packing for spheres of equal size uses approximately 74% of the volume $(C_k = 0.74)$, while the densest packing for cubes of equal size can use 100% of the space. It has been shown that organic crystals with irregular molecular shapes tend to have packing coefficients that vary from ca. 0.64 to 0.77, with structures characterized by voids and protuberances producing the lowerend values. ²⁹ By contrast, extended crystal structures based on coordination bonds between

relatively rigid spacers (such as MOFs) can sustain large amounts of empty space with C_k values as low 0.10 (i.e., void volumes of 90%). While C_k values do not give an indication of how the free volume is distributed in the unit cell, at a first approximation it seems reasonable to expect that packing coefficients should be inversely correlated with internal dynamics. If this were the case, then one would expect a rough inverse correlation between packing coefficient and rotational rate and the data points should cluster along a diagonal that goes from the top-left to the bottom-right in Figure 5. However, ambient temperature k_r values on the vertical axis as a function of the calculated C_k for 31 amphidynamic crystals with 36 crystallographically distinct rotational sites fail to follow the expected trend, indicating that there are other factors to consider.

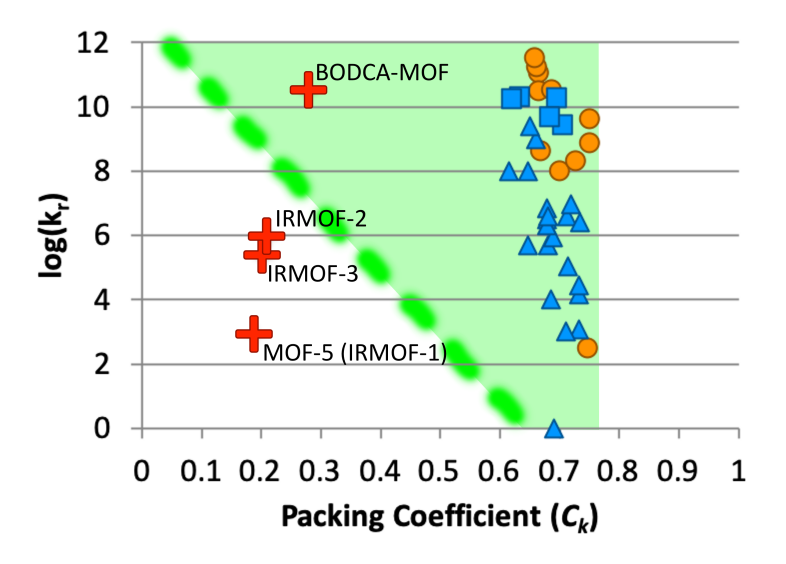


Figure 5. a) A scatter plot of the room-temperature Brownian rotational velocities (k_r , s^{-1}) of amphidynamic crystals as a function of their packing coefficients (C_k). The different symbols correspond to four different sets of amphidynamic crystals: (I) The "plus" signs correspond to MOFs; (II) Circles are the high symmetry rotators; (III) Triangles are molecular rotors with phenylene rotators and stators derived from a trityl or triptycyl motif, and (IV) squares correspond to supramolecular rotors.

Figure 5 includes packing coefficients from four different types of amphidynamic crystals that have well (or reasonably well) characterized ambient temperature (300 K) rotational dynamics. These include (I) MOF rotors (crosses), (II) molecular rotors with rotators that have a rotational symmetry order higher than C₂ (circles), (III) molecular rotors with phenylene or heterocyclic rotators and stators derived from a trityl or triptycyl motif (triangles), and (IV) molecular rotors with supramolecular axles (squares).

We obtained each of the packing coefficients with molecular volumes determined with modeling software^{32,33} and the unit cell volumes from their single crystal X-ray diffraction structures. Rotational Brownian motion in crystals, k_r, was measured using three variable temperature (VT) solid-state NMR methods depending on the rates (or frequencies, in units of s⁻ ¹, or Hz) at which the moving groups exchange between different sites along their rotational potential. 19 Motions occurring with slow exchange rates (ca. 100 to 10,000 Hz) can be obtained by VT ¹³C CPMAS NMR when the different sites have sufficiently different chemical shifts. Rotational exchange rates in the regime of 10 kHz to 10 MHz can be obtained by taking advantage of line shape analysis of the spectra obtained by quadrupolar echo ²H NMR using ²Hlabeled samples. This is a powerful method, as it provides information not only on the site exchange frequencies but also the trajectories of motion. Finally, the most convenient method to measure rotational dynamics in the high frequency regime of ca. 10 MHz to >600 MHz is the VT measurements of spin-lattice relaxation of magnetic nuclei (¹H, ²H, ¹³C, ¹⁹F etc.) in the rotator. After gathering exchange rate (k_r) data from these techniques as a function of temperature, one can use the Arrhenius equation, $k_r = A \exp(-E_a/RT)$, to determine activation energies (E_a) and pre-exponential factors (A), which make it possible to estimate the rate of rotation at 300K. While the activation energy represents the height of the barrier along the rotational potential, the

pre-exponential factors represent an attempt frequency, which is related to the frequency of the torsional mode that causes oscillations at the bottom of the potential energy well. For small rotators, the pre-exponential factor has values on the order of 10^{11} - 10^{12} s⁻¹.

It is clear from Figure 5 that there are significant deviations from the expected behavior with data points roughly segregated on the high and low packing density regions. Molecular and supramolecular crystals cluster on the right side of the plot, covering packing coefficients that vary from ca. 0.6 to 0.8 and rotational frequencies that range from static to those that are close to the upper theoretical limit, given by the pre-exponential factor, ca. $k_r \approx A = 10^{11} - 10^{12} \text{ s}^{-1}$. By contrast, the molecular rotors incorporated as MOF pillars studied by our group so far cluster on the left side of the figure. One can see that despite MOFs having the lowest packing coefficients ($C_k < 0.3$), the data points reveal examples of MOF kinetics that range from slow ($k_r \approx 10^3 \text{ s}^{-1}$) to moderate ($k_r \approx 10^6~\text{s}^\text{-1}$) to ultrafast ($k_r \approx 5 \times 10^{11}~\text{s}^\text{-1}$) rotation. To explain these differences, one must consider that in addition to intermolecular forces, which determine the energetics of rotation in terms of free volume, axial symmetry, or gearing motions, one of the key parameters in determining rotational dynamics is the intrinsic rotational potential of an isolated rotator. When intra-molecular and inter-molecular factors are analyzed together, one can recognize two general regimes of dynamic behavior. These correspond to the limits of (A) activation control, when rotational motion is limited by the intrinsic barrier of the rotator, and (B) diffusion control, when rotational motion is limited by intermolecular hindrance arising from near neighbors in the lattice, which can be seen as a measure of crystal fluidity (see Section 8 below).

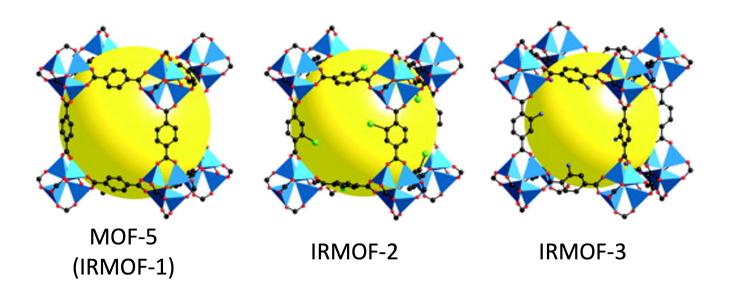


Figure 6. Structure of cubic isoreticular metal organic frameworks (IRMOF) with substituted benzene dicarboxylate linkers and zinc oxide clusters.³⁴

6. Activation-Controlled Rotation in Amphidynamic Metal Organic Frameworks

While it should be possible to prepare metal-organic frameworks that cover the range of rotorrotor distances and interactions shown in Figure 4, the MOFs in Figure 5 were selected with the expectation that they would have sufficiently large free volumes for their rotators to have no steric hindrance. Their structures are based on zinc oxide clusters linked by aromatic dicarboxylate rotators $[Zn_4(rotatorC_2O_4)_3]$ related to the iconic MOF-5, which is also known as IRMOF-1 (Figure 6). Importantly, all of these structures have empty volumes that are greater than the volumes of revolution of the rotator, and the four IRMOFs included in Figure 5 are a good example of the conditions shown in Figure 4d, with $C_k < 0.3$. Lacking steric hindrance, their rates of rotation vary significantly because those rates are determined by intrinsic electronic barriers. It was first shown that the loss of []-conjugation between the two coplanar carboxylates and the central phenylene at the rotational transition state of IRMOF-1 gives rise to a relatively high energy barrier of 11.3 kcal/mol. ²⁰ This high barrier and a pre-exponential factor of ca. 1.6 × 10^{12} s⁻¹ lead to rates of rotation of ca. 10^4 s⁻¹ near ambient temperature. It was subsequently shown that changes in the intrinsic rotational potential of the aromatic rotators are altered by substituents. In that vein, a bromine substituent on the phenylene rotator in the case of IRMOF-2

studied by Winston *et al.*³⁵ showed a 300 K rotational frequency that was increased by two orders of magnitude to ca. 2.6×10^6 s⁻¹. This increased rotational frequency is the result of

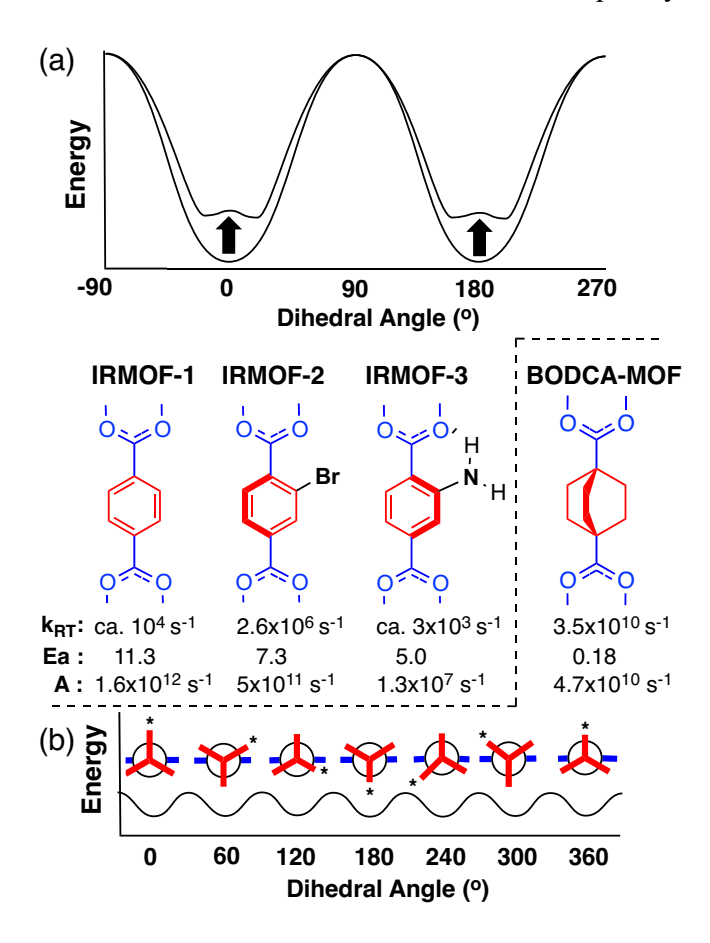


Figure 7. (a) Differences in rotational frequencies of IRMOF-1, IRMOF-2 (2-Br) and IRMOF-3 (2-NH₂) can be assigned to changes in the barrier height that result from the ground state steric destabilization by the *ortho*-substituents, which prevent planarization and full □-conjugation, and changes in the low pre-exponential factor in the case of IRMOF-3 (see text). (b) Removal of □-conjugation and a six-fold rotational symmetry potential in the aliphatic bicyclo[2.2.2.]octane dicarboxylate rotator in the case of BODCA-MOF reduces the activation energy (0.12 kcal/mol) to values that are much lower than thermal energies near 300 K (*ca.* 0.6 kcal/mol).

having a similar pre-exponential factor ($A = 5 \times 10^{11} \text{ s}^{-1}$) and a lower barrier of $E_a = 7.3$ kcal/mol. However, as suggested in Figure 7a, the smaller barrier is the result of the ground state

destabilization that occurs from the steric congestion around the metal centers, which prevents full conjugation between the 2-bromophenylene and the carboxylate groups in the ground state. The effect of a 2-aminophenylene in the case of IRMOF-3 was shown to be more complex. 36 A very slow rotational frequency of ca. 3×10^3 s $^{-1}$ at 300 K was estimated despite a lower activation barrier of only $E_a = 5.0$ kcal/mol as a result of a lower pre-exponential factor, $A = 1.3 \times 10^7$ s $^{-1}$, which is about 3 orders of magnitude smaller than those of IRMOF-1 and IRMOF-2. While the lower barrier seems to be the result of a substantial ground-state destabilization, the low pre-exponential factor reflects an attempt frequency for rotation that is not uniquely determined by the frequency of the thermal oscillations of the rotator, but is instead modulated by the need to cleave the N-H $^{++}$ O=C hydrogen bond, which becomes a rotational rate-limiting step.

That the electronics of the intrinsic energetic potential are responsible for the rotational frequency of the benzenedicarboxylates in the IRMOF series could be shown by the design and synthesis of a new structure with a saturated bicyclo[2.2.2]octanedicarboxylate (BODCA) rotator (Figure 7b).²¹ In addition to the removal of a significant electronic barrier, the BODCA linker has a three-fold axis of symmetry, which combines with the two-fold rotational symmetry of the carboxylate to generate a six-fold rotational potential, as shown in the bottom of Figure 7b, where Newman projections of the rotamers are shown along with the corresponding small changes in energy. The rotational dynamics of samples of BODCA-MOF measured between 298 K and 6 K revealed a barrier of only 0.18 kcal/mol and a pre-exponential factor of 4.7 × 10¹⁰ s⁻¹, which makes it the first example of a crystalline solid with structural components that undergo barrierless rotation over a broad temperature range. While a low intrinsic barrier and the lack of intermolecular hindrance may suggest high temperature gas phase-like rotation, molecular

dynamics simulations confirm that BODCA-MOF behaves as a diffusion-controlled molecular rotor. With rotational barriers that are smaller than thermal energies, Brownian rotation is determined by the coupling of angular motion with normal modes and lattice vibrations, which can have the same or different phase, such that motion occurs in a random fashion with no sustained directionality and angular momentum.

7. Diffusion-Controlled Rotation in Close Packed Molecular Crystals

Disubstituted acetylenes are among the most versatile design elements for the construction of molecular rotors. Taking advantage of robust synthetic methods based on transition-metal-catalyzed coupling reactions and nucleophilic additions with acetylide anions, alkynes can be used to link a wide variety of stators and rotators while also providing them with an axle for

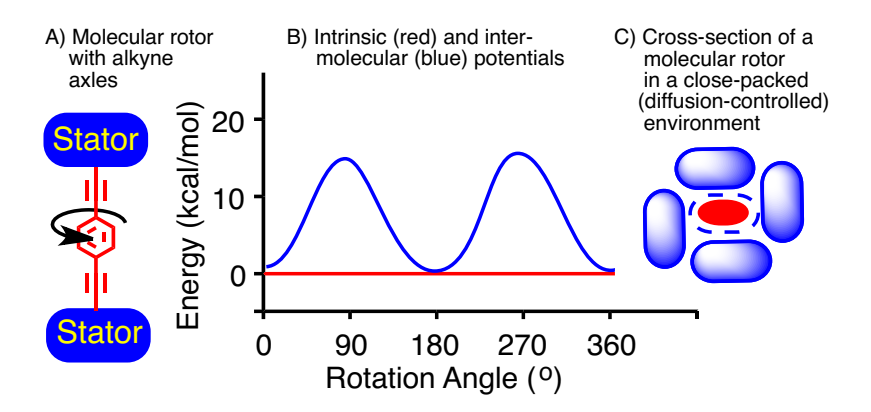


Figure 8. Molecular rotors with alkyne axles have a (nearly) barrierless intrinsic potential, which makes their solid-state rotational dynamics fall in the diffusion-controlled regime; Barriers depend on the rigidity of the environment.

rotation. Importantly, acetylenes have orthogonal \square -orbitals with an effective cylindrical symmetry, such that rotation about triple bonds causes no changes in ground state energetics³⁷ (Figure 8, red line) even when the rotator and the stator at the two ends are linked through sp²-

hybridized carbon atoms. Based on these characteristics, many molecular rotors with alkyne axles are based on a simple design where there is a central rotator co-axially linked to bulky groups that play the role of the stator (Figure 8). Molecular motion in such close-packed molecular crystals is hindered by contacts between the otherwise freely moving rotator and neighboring molecules in the lattice, which form a relatively hard boundary that conforms to the van der Waals surface of the rotator. As indicated in Figure 8, rotational motion under these conditions falls in a diffusion-controlled regime where local volume fluctuations are needed for rotation to take place.³⁸

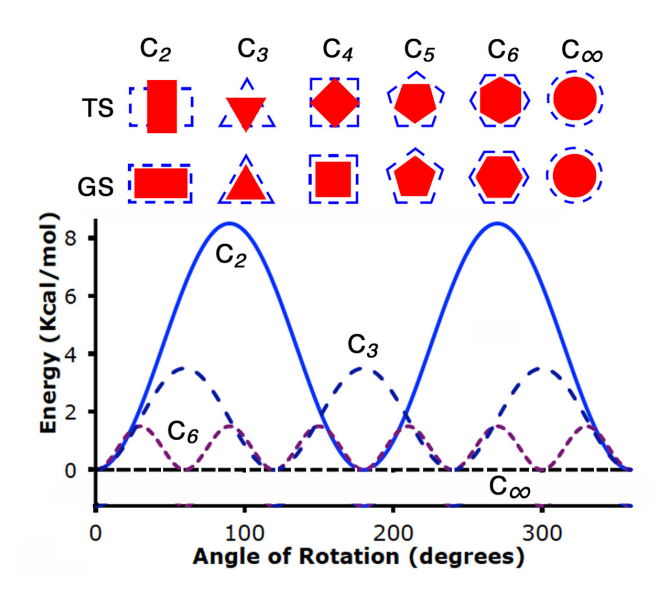


Figure 9. (Top) Overlap between the cross sections (solid red) and van der Waals surface boundary (dotted blue) of a set of hypothetical polyhedral molecular rotators with axial symmetry order varying from C_2 to C_{∞} in their rotational ground state (GS) and transition state (TS). (Bottom) Changes in the potential energy profile for rotators with C_2 , C_3 , C_6 and C_{∞} rotational axis (adapted from reference 24).

8. Variations in the Structure of the Rotator: Axial Symmetry Order²⁴

Based on simple geometric arguments, we suggested a few years ago that the extent of overlap between the shape of the rotator and its volume of revolution should be a key factor in determining rotational dynamics. Since the crystal environment is expected to conform to the shape of the rotator, the corresponding overlap will depend on the size, shape, and the axial symmetry order of the rotator.²⁴ As illustrated in Figure 9, a set of polygonal rotators with a given rotational symmetry order C_n will have periodic rotary potentials with energy profiles that have "n" minima and "n" maxima, angular displacements of 360/n °, and barriers that become smaller as the shape of the rotator approaches the shape of a cylinder, when $n \rightarrow \infty$. Ideal potential energy surfaces will have a periodic dependence on rotational angle (\square) given by E(\square) = $\frac{1}{2}$ E₀ (1-cos n). One of the most interesting applications of rotational symmetry can be found in the design of the bacterial flagellum³⁹ where the symmetry order of the flagellar rotator (n_{Rot} = 24-26) does not match the symmetry of the stator ($n_{Stat} = 34-36$), giving rise to a potential energy profile where the effective symmetry is the product of the two, $n_{Effective} = n_{Rot} \times n_{Stat}$, such that combined they approach a smooth cylinder-like surface. Furthermore, an increase in the number of "n" results in greater directional resolution that may be addressed with external stimuli when a suitable dipole is included in the rotator structure. 40,41 Similarly, rotators with n > 2 and vertices extending in a radial manner may be envisioned as structural elements for the design of ntoothed molecular gears, as shown for the 3-toothed triptycene gear in Figure 3.

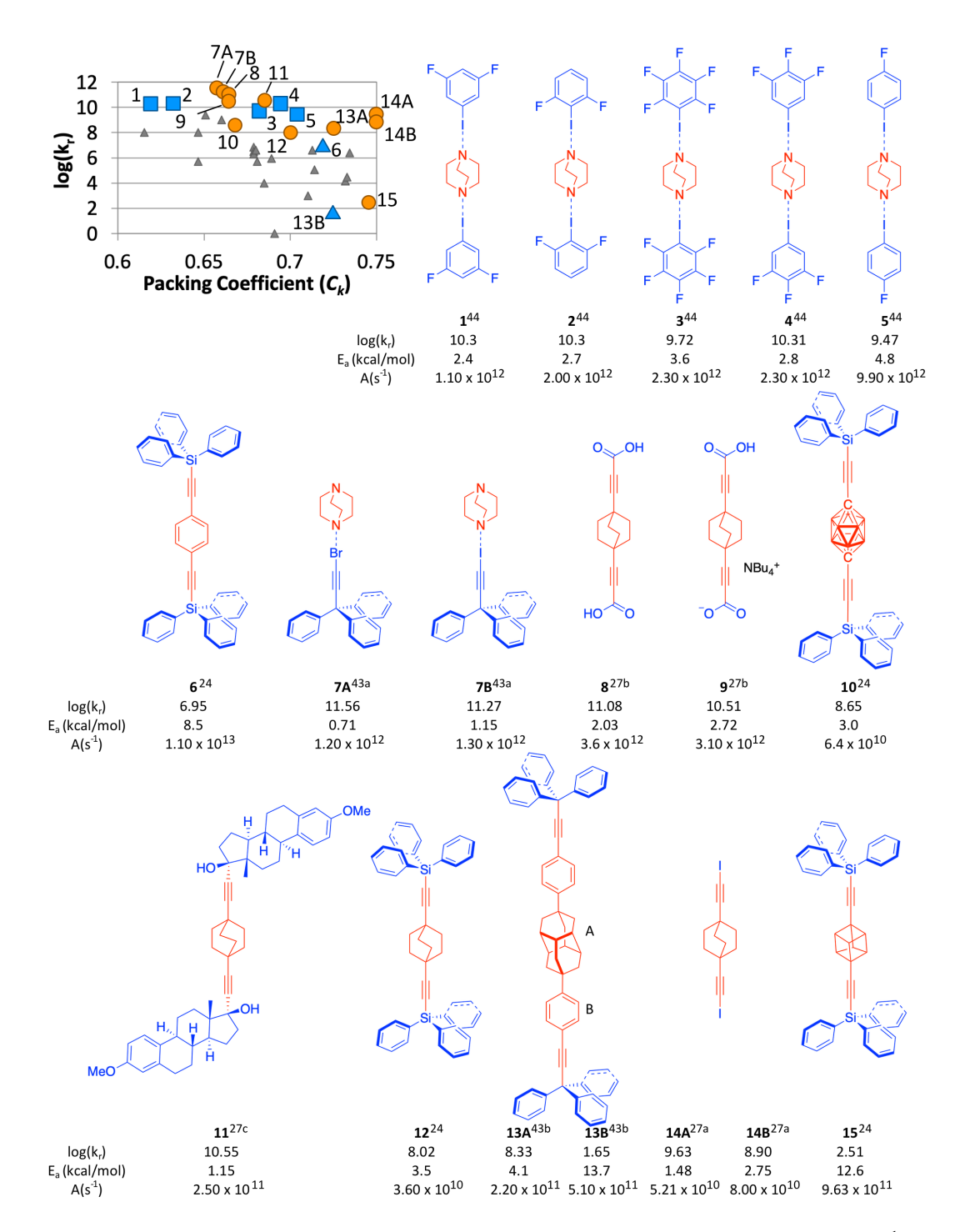


Figure 10. Scatter plot of the ambient-temperature Brownian rotational velocities (k_r , s^{-1}) of amphidynamic crystals of molecular and supramolecular rotors with high axial symmetry order as a function of their packing coefficients (C_k). Squares correspond to supramolecular rotors, circles to other high-symmetry rotators, and triangles to molecular rotors with phenylene rotators

and trityl or triptycyl stators. Numbered rotor structures are shown with their literature reference as a superscript as well as their 300 K rotational velocities $[log(k_r)]$, activation barriers (E_a) , and pre-exponential factors (A). Both the diamantane and the phenylene in compound 13 rotate: they are labeled 13A and 13B, respectively. Molecular rotor 14 crystallizes in two distinct sites that are labeled 14a and 14b.

Figure 10 shows a series of halogen (1-5, 7 and 14) and hydrogen (8-9) bonded supramolecular rotors, as well as molecular rotors with steroidal (11) or triaryl-substituted stators (6, 10, 12, 13 and 15) that are linked to high axial symmetry rotators. Among them, a homologous set of with triphenylsilyl stators and alkyne axles have rotators with an increasing rotational symmetry order (C_n) . These include phenylene rotor 6 (C_2) , cubyl rotor 15 and BCO rotor 12 (C_3) , and a paracloso-dodecacarborane rotor $10 (C_5)$. It was shown that crystals of the two-fold symmetric phenylene rotor 6 have a barrier of 8.5 ± 2.5 kcal/mol and a rotational frequency of 9 MHz at 300 K. Increasing the symmetry to BCO 12 decreases the barrier to 3.5 ± 0.2 kcal/mol while increasing the room temperature rotational frequency by an order of magnitude, to 105 MHz. The trend continues with the five-fold symmetric carborane rotor 10, which was shown to have an even lower barrier of 3.0 ± 0.1 kcal/mol and an increase in its room temperature rotation to 446 MHz. An exception was encountered with the smaller three-fold symmetric cubyl rotor 15. This relatively small rotator displays an unexpectedly slow rotational frequency of only 320 Hz at 300 K due to specific packing interactions wherein a phenyl group from an adjacent triphenylsilyl stator is packed exceptionally close to the rotator in a way that obstructs rotation and results in an unusually high activation energy of 12.6 kcal/mol.²⁴

It should be pointed out that high symmetry rotators may adopt rotationally disordered structures that increase the average symmetry of their crystal space group. For example, crystal

structures with BCO rotators are often solved with an inversion center that is not present in the BCO structure, but that can be satisfied on average by a local disorder where the BCO group adopts two positions related by a 60° rotation with equal probability. Usually observed at higher temperatures, this disorder transforms the point group of the BCO from a local D_{3h} into an average D_{6h} , and the rotational axis from C_3 to C_6 . An example is shown in Figure 11 with the halogen bonded supramolecular rotor **3** formed with one equivalent of 1,4-diazabicyclo[2.2.2]octane (DABCO) and two of pentafluroiodo benzene. The structure solution of the X-ray diffraction data displays increasing rotational disorder in going from 103 K to 200 K, with a phase transition occurring between 220 K and 250 K.

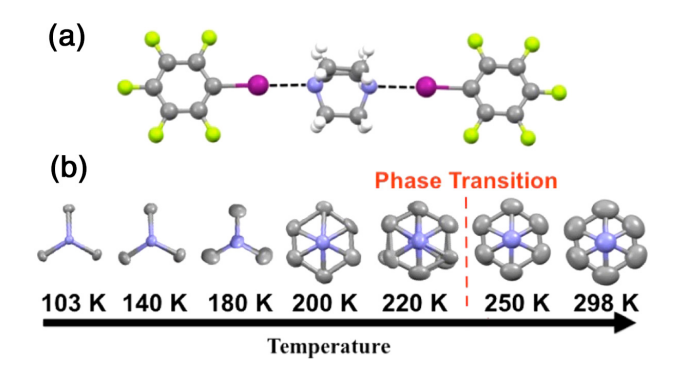


Figure 11. (a) Crystal structure data of a representative supramolecular rotor based on halogen bonding between 2,4-diazabicylo[2.2.2]octane (DABCO) and pentafluoro-iodobenzene. (b) Crystal structures obtained at increasing temperature display increasing rotational disorder of the DABCO group.

The three-fold symmetry and the relatively spherical shape of the BCO rotator make it an ideal rotator for creating systems with low rotational barriers in close packed crystals when linked to the stator by a barrierless alkyne linkage or a supramolecular bond. In fact, all of the supramolecular high symmetry rotors highlighted in Figure 10 feature a BCO rotator and they all have ambient temperature rotational frequencies greater than 200 MHz with activation energies

that are less than 5 kcal/mol.^{27,43,44} Additionally, most of these crystals have packing coefficients of 0.65 or greater, so that their fast dynamics are not the result of a lower density environment, but rather the result of a volume-conserving rotational motion.²⁴

8. Variations in the Structure of the Stator: The Emergence of "Crystal Fluidity"

In order to explore the effects of structural variations in the stator, we took advantage of a synthetically accessible 1,4-phenylene rotator and two sets of stator structures that are relatively easy to obtain and modify. One set consists of triptycyl molecular rotors prepared by the installation of two co-axial 9-triptycyl acetylenes, prepared by the Diels-Alder addition of

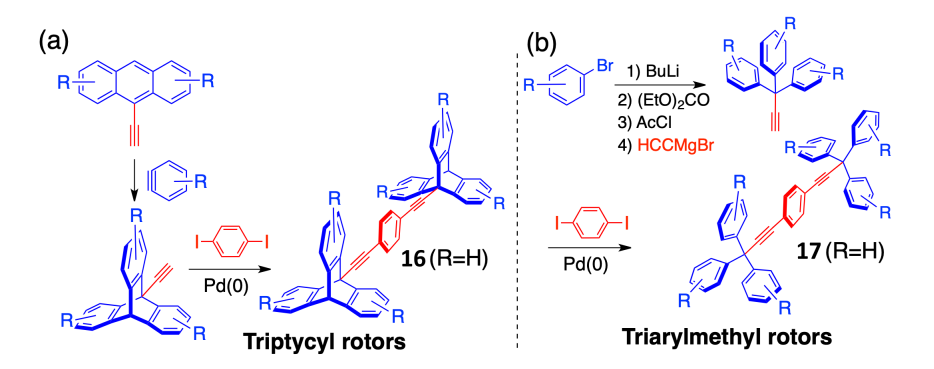


Figure 12. (a) General synthetic pathway for rotors containing triptycyl stators: ethynylanthracenes undergo a Diels-Alder cyclization with a benzyne to form the triptycyl stator before being coupled to the rotator. (b) General synthetic pathway for rotors containing trityl stators: diethylcarbonate and a bromobenzene are used to form the trityl stator before being

benzynes to ethynylanthracenes, onto 1,4-dihalogenated benzenes by a Pd(0)-mediated Sonogashira reaction (Figure 12a).⁴⁵ The other is based on triarylmethyl molecular rotors obtained in a similar manner by taking advantage of readily available triarylacetylenes (Figure

coupled to the rotator.

12b). 46 The relatively rigid three-fold symmetric triptycyl and triarylmethyl stators were expected to help guide the packing structure and the integrity of the crystal lattice while providing the conditions needed for the mobility of the rotator, which might include the steric shielding hypothesized in Figure 4c. The starting point to explore this concept began with molecular rotors 16 and 17, with unsubstituted triptycyl and triarylmethyl groups (Figure 12, R = H), which turned out to be robust crystalline solids with their rigid rod-like structures adopting a low symmetry order (space group P1-bar), which would ensure that all phenylenes rotate on the same plane of the crystal, as it would be desired for a dipolar array. 45,46 However, rather than leaving a low packing density region in the area of the rotator, crystals of molecular rotor 16 grown from *meta*-xylene incorporated the solvent into the structure. On the other hand, triarylmethyl molecular rotor 17 could be obtained either solvent-free from CH₂Cl₂, or with solvent incorporated when grown from benzene. 47 It was shown that crystals of molecular rotor 17 undergo a reconstructive phase transition upon solvent removal. A stark difference between the crystals of molecular rotors 16 and 17 is that, while the former is essentially static, VT solid state ¹³C CPMAS NMR showed that the latter undergoes ambient temperature rotational site exchange in the kilohertz regime with activation energies in the range of 12-15 kcal/mol and preexponential factors of ca. 10^{14} s⁻¹. A comparison of their packing coefficients revealed that crystals of 16 and 17 have similar packing densities ($C_k = 0.7$), demonstrating that the same average amount of empty space does not result in similar rotational freedom. A simple analysis of the cross section of the phenylene rotators in crystals of 16 and 17 in Figure 13a confirms that there are no significant differences in the volume available. In fact, the primary reason for their different dynamic behavior was suggested by subsequent computational modeling of the two

crystal forms of triarylmethyl structure 17, which revealed that rotation in the crystal lattice relies on conformational degrees of freedom available to the triphenylmethyl groups. It was

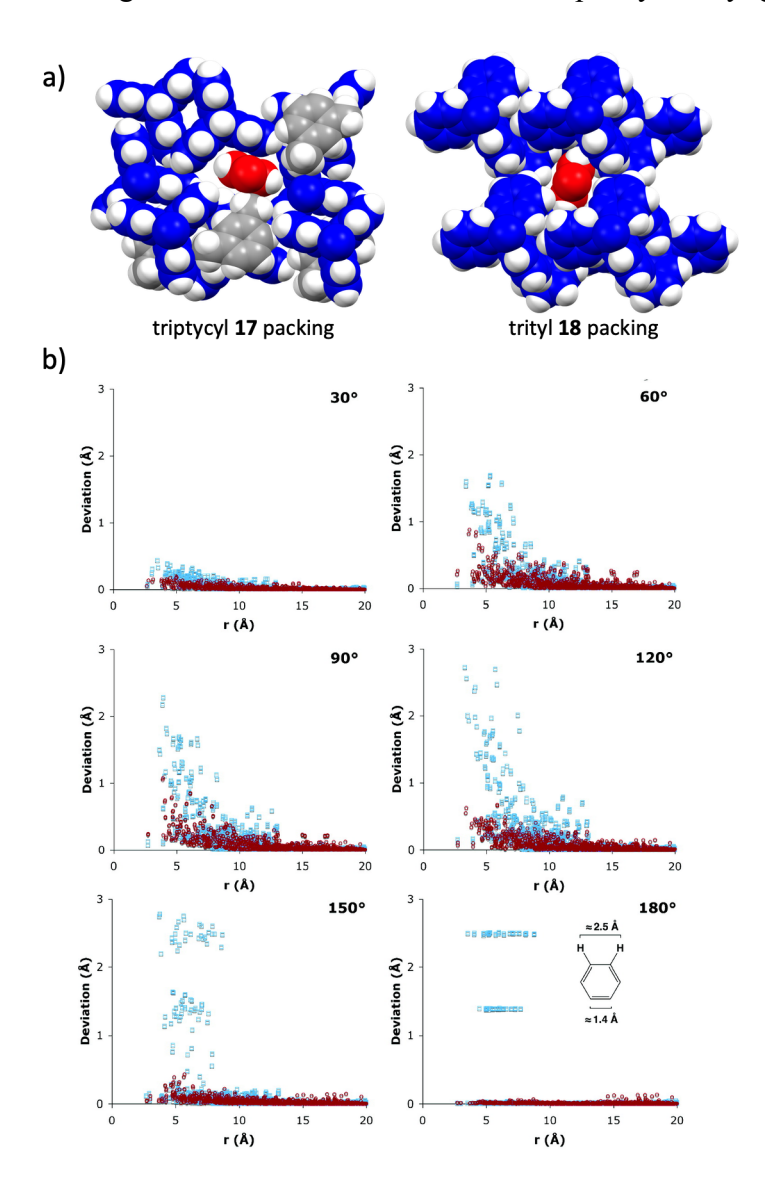


Figure 13. (a) Cross sections of the crystal structures around the phenylene rotators of triptycyl and trityl rotors **16** and **17** showing the lack of free volume surrounding each phenylene rotator. b) Calculated displacement of neighboring atoms surrounding a reference rotator as it undergoes a 180° flip. The phenyl groups corresponding to near neighbor trityl stators are shown in red and those corresponding to the solvated crystal, including benzene molecules, are shown in blue.

Blue atoms undergoing displacements of 1.4 Å and 2.5 Å correspond to benzene molecules undergoing a correlated rotation with the central phenylene (adapted from reference 38). discovered that all the phenyl groups in the crystal lattice oscillate about their equilibrium positions, creating transient cavities that enable the central phenylene to rotate.³⁸ The magnitude of the conformational motions and the corresponding cavity fluctuations can be qualitatively appreciated by tracking the displacement of every atom in the surrounding phenyl groups as a function of the rotational angle during a 180° ring flip of the central phenylene. This is shown in Figure 13b with data corresponding to rotational angles of 30°, 60°, 90°, 150°, and 180°, where each point corresponds to a single atom in the neighboring trityl groups and also benzene molecules in the case of solvated structure (data points shown in blue). One can see that rotation of the central phenylene is accompanied by a significant rearrangement of the neighboring lattice with the maximum observed at the rotational transition state of 90° and a return to the equilibrium positions after 180°, with the exception of the benzene molecules that undergo a correlated 60° rotation. While the simulations of analogous molecular rotors would be needed to confirm it, we propose that the type of lattice fluctuation displayed by the nearby atoms, or crystal fluidity, is likely to play an important role in the rotational dynamics of close-packed crystalline molecular rotors.

It is worth highlighting that the ambient temperature dynamics of analogs of 17^{46} with a bridging azobenzene (18^{48e}), a gold (I) phosphane extended axle (19^{48d}), mixed trityl and tryptycene stator (20^{48f}), imine-extended rotator (21^{48g}), polar fluorinated phenylenes (22^{48b} and 24^{48a}), N-heterocyclic rotators (23^{48c}) and a dual rotor with a pentypticene core (25^{48h}) display dynamics that range over 3 orders of magnitude, from the 10^3 s⁻¹ to the 10^6 s⁻¹ regime, even though their packing coefficients are narrowly clustered between 0.65 and 0.74 (Figure 14).⁴⁸

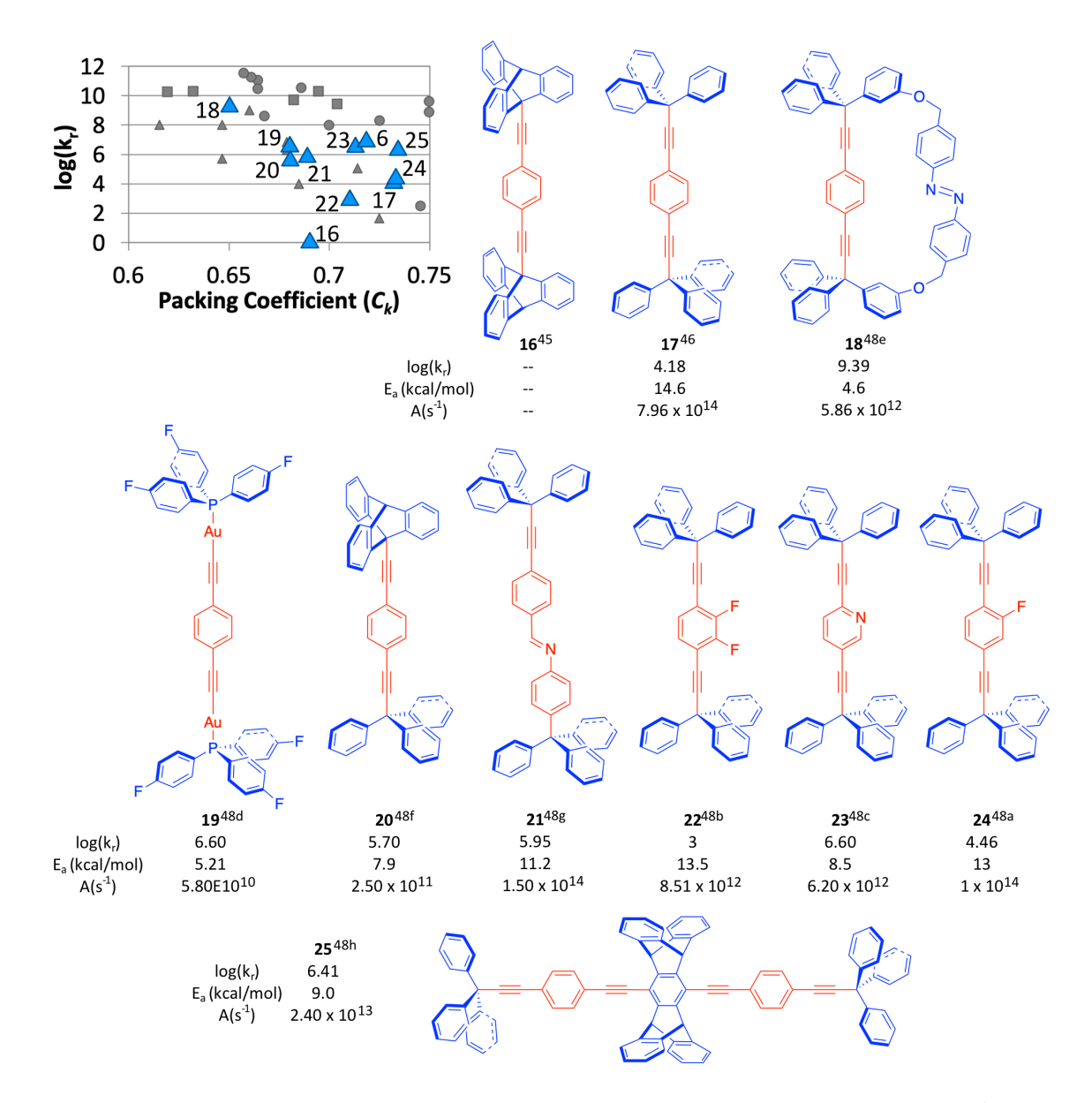


Figure 14. Scatter plot of the ambient-temperature Brownian rotational velocities (k_r, s^{-1}) and packing coefficients of amphidynamic crystals with unsubstituted triptycyl and/or trityl stators shown as blue triangles. Numbered rotor structures are shown with their literature reference as a superscript as well as their 300 K rotational velocities $[log(k_r)]$, activation barriers (E_a) , and preexponential factors (A). Compound **6** is shown in Figure 10.

We hypothesize that crystal fluidity accounts for the lack of a simple correlation between C_k and k_r displayed in Figure 5, with points that occur above the diagonal signaling the presence of internal degrees of freedom that cause volume fluctuations where rotation can take place.

9. Engineering Crystal Fluidity with Expanded Stators.

The significance of crystal fluidity is also supported by results with molecular rotor 26 with peripheral tert-buryl groups that increase the rotational frequency of the central phenylene up to 10⁸ s⁻¹ by increasing the number of degrees of freedom in the structure. ^{50a} Similarly, triptycyl rotor 27 (Figure 15), where the size of the stator was extended by the addition of peripheral methyl groups, ⁴⁹ which intended to prevent the interdigitation of adjacent molecules in the lattice while promoting a layered packing motif. While the desired solid-state architecture was achieved, the space formed by adjacent rotors was relatively large and stable crystals could only be obtained with the inclusion of bromobenzene, which was used as the solvent of crystallization (Figure 15). Despite relatively tight packing, phenylene rotation in crystals of 27 occurred with a relatively low activation energy of 4.4 kcal/mol, which leads to ambient temperature rotational rates of ca. 1.1×10^9 s⁻¹. Considering the disposition of the solvent and rotator revealed by the cross section in Figure 15, it seems very likely that rotation in the case of 27 may involve the correlated motion of the solvent molecules, implying that the solvent contributes a certain level of fluidity to the amphidynamic crystal. Furthermore, a number of expanded stators based on trityl motifs have also been investigated. ⁵⁰ Trityl rotors with *meta*-methoxy, 3,5-di-*tert*-butyl, 2,5-diphenyl, and para-trialkylsilyl substituents have all been explored and shown to have both faster dynamics and lower packing coefficients than the unsubstituted compound 17. These

compounds lend additional credibility to the idea that added conformational degrees of freedom are likely to increase the fluidity of the lattice.

10. The Dynamics of Fluid Crystalline Rotors

An additional powerful example of this concept emerged from the observation of dendritic rotor 28, which was designed to test the effects of an expanded stator on the dynamics of the central rotator (Figure 15).⁵¹ Recognizing that this rotor has three separate positions where rotation could be observed as a manifestation of crystal fluidity, selectively ²H-labeled samples were prepared to determine the dynamics of the central phenylene shown in red, the branch phenylenes shown in green, and the peripheral phenyl groups that are shown in blue. Molecular rotor 28 is unique because the stator is defined by the sigma bonding framework of the structure while all of the bulky aromatic groups are mobile. All three positions display apparent preexponential factors and activation energies with values that are over 10¹⁵ s⁻¹ and 13 kcal/mol, respectively, which give rise to ambient temperature rotation in the MHz regime. It should be noted that these pre-exponential factors exceed the 10^{12} s⁻¹ maximum that is expected for an elementary process.⁵² This was observed in another case where the steep slope of the Arrhenius plot and a large pre-exponential factor were interpreted as the result of softening of a rigid glass on its way to become a rotational fluid.⁵³ Part of this increased fluidity is due to the mobility of the three elements, but it is also enabled by a large amount of disordered solvent that allows for a packing coefficient of ca 0.68.

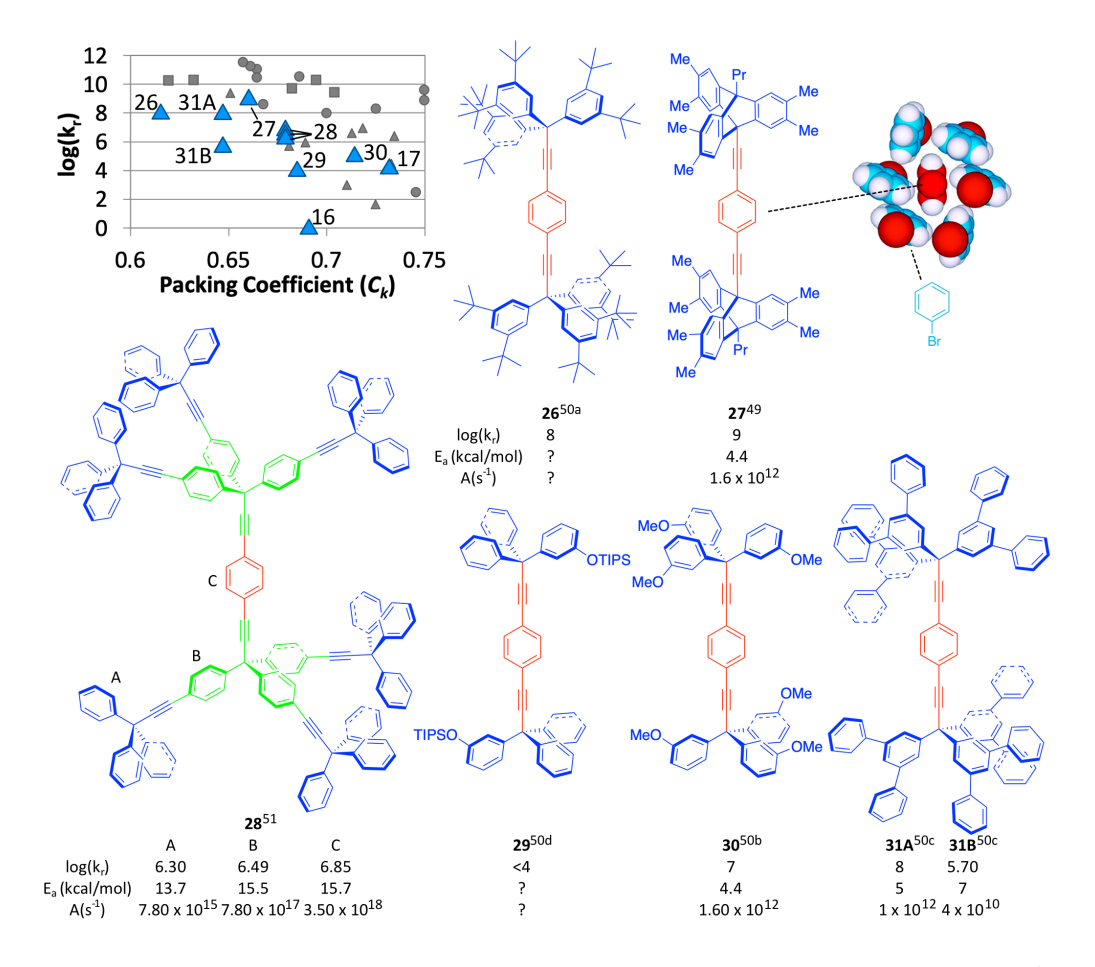


Figure 15. Scatter plot of the ambient-temperature Brownian rotational velocities (k_r, s^{-1}) and packing coefficients of amphidynamic crystals with expanded stators highlighted as triangles. A view down the rotational axis of the phenylene in **27** suggest that correlated motion of surrounding bromobenzene molecules may be responsible for the fast rotation observed. Fast rotation was measured at all three sites in dendritic rotor **28**. Compound **31** crystallizes with distinct crystallographic sites **31A** and **31B**. Numbered rotor structures are shown with their literature reference as a superscript as well as their 300 K rotational velocities $[log(k_r)]$, activation barriers (E_a) , and pre-exponential factors (A). Unsubstituted triptycyl and trityl model systems **16** and **17** are shown along with their dynamics in Figure 14.

11. Conclusions

A simple approach for the design of molecular rotors based on the volume of revolution and center-to-center distance between neighboring rotators suggests that rotational dynamics should be governed by (1) the creation of free space, (2) the use of volume-conserving shapes, like spheres or cylinders, or (3) gearing motions when adjacent rotators are interdigitated. However, for general structures lacking the latter two properties, a comparison of average free volume measured in terms of packing coefficient (C_k) and ambient temperature Brownian rotational velocities revealed that this simple approach ignores several key aspects of the behavior of amphidynamic solids. The survey presented herein reveals two sets of governing principles: one applies to MOFs and extended solids with rotations enclosed in large empty cavities and the other determines the rotational dynamics of close-packed molecular crystals. It can be shown that rotational motion in the solid state occurs in an activation-controlled regime when there is sufficient free volume for rotational dynamics to depend on the intrinsic (gas phase) electronic barrier about the bond (axle) that links the rotator and the stator. For □-conjugated systems, the energy cost of breaking conjugation can lead to very high barriers, which can be reduced by taking advantage of structural factors that can destabilize the ground state. The use of nonconjugated rotators with high orders of rotational symmetry can lead to ultralow intrinsic barriers and ultrafast rotation. By contrast, molecular crystals do not benefit from large amounts of free volume and their dynamics become diffusion-controlled, such that rotational barriers are determined by how well crystal packing can accommodate the motion of the rotator. For spherically shaped, volume-conserving rotators such as bicyclo[2.2.2]octane, 21 1,12dicarbaclosocarborane, ²⁴ and C₆₀, ⁵⁴ there is a good overlap between the volume of revolution and the volume of the packing cavity that contains it, such that fast dynamics and low barriers can be

observed despite a relatively high packing coefficient. For molecular rotators with non-spherical

shapes, such as 1,4-phenylenes, Brownian dynamics are determined by whether or not the crystal

environment around the rotator can re-accommodate to create transient cavities for rotation to

occur, a property that we have termed "crystal fluidity." The importance of crystal fluidity is

strongly supported by the comparison of molecular rotors with vastly different degrees of

torsional freedom.³⁷ For example, molecular rotors based on conformationally flexible

triphenylmethyl stators are significantly more dynamic than analogous molecular rotors based on

rigid triptycene stators. The effect of crystal fluidity is highlighted by the fast rotational motion

of all phenylene branches in dendritic rotors with local conformational flexibility.⁵¹ The survey

presented in this perspective revealed a new set of governing design principles for crystalline

molecular rotors, which had previously been centered around the creation of free space. The

concept of crystal fluidity will inform the future design of crystalline molecular rotors and

amphidynamic crystals, by considering the use of flexible frameworks in addition to the creation

of empty space. It is reasonable to expect that improvements in the design and preparation of

molecular rotors will make it possible to improve their performance in a number of promising

applications. 15,55

AUTHOR INFORMATION

Corresponding Author

*Email: mgg@chem.ucla.edu

33



Miguel A. Garcia-Garibay research interests cover various aspects of organic solid state chemistry, including solvent-free synthesis, quantum chain reactions, reactive intermediates, spectroscopy with nanocrystals, and crystalline molecular machines.



Morgan Howe joined the Garcia-Garibay group in 2015, where she is currently pursuing research involving the luminescence and dynamics of amphidynamic crystals.

Funding Sources

This work has been supported by National Science Foundation grants DMR-1700471 and MRI-1532232.

ACKNOWLEDGMENT

We thank many students and postdocs at UCLA and many collaborators for numerous contributions to the work presented here.

REFERENCES

1 a) Iwamura, H.; Mislow, K. Stereochemical Consequences of Dynamic Gearing. *Acc. Chem. Res.*, **1988**, *21*, 175-182. b) Ōki, M. Unusually high barriers to rotation involving the tetrahedral carbon atom. *Angew. Chem. Int. Ed. Engl.*, **1976**, *15*, 87-93. c) Mislow, K. Stereochemical consequences of correlated rotation in molecular propellers. *Acc. Chem. Res.*, 1976, 9, 26-33. d) Anelli, P.L.; Spencer, N.; Stoddart, J.F. A molecular shuttle. *J. Am. Chem. Soc.*, **1991**, *113*, 5131-5133. e) Kelly, T.R.; Bowyer, M.C.; Bhaskar, K.V.; Bebbington, D.; Garcia, A.; Lang, F.; Kim, M.H.; Jette, M.P. A molecular brake. *J. Am. Chem. Soc.*, **1994**, *116*, 3657-3658. f) Bedard, T.C.; Moore, J.S. Design and synthesis of molecular turnstiles. *J. Am. Chem. Soc.*, **1995**, *117*, 10662-10671. g) Gakh, A.A. *Molecular devices: an introduction to technomimetics and its biological applications*; Wiley: Hoboken, NJ, USA, 2018. h) Jimenez-Bueno, G.; Rapenne, G. Technomimetic molecules: synthesis of a molecular wheelbarrow. *Tetrahedron Lett.* **2003**, *44*, 6261-6263.

2 a) Mislow, K. Stereochemical consequences of correlated rotation in molecular propellers. *Acc. Chem. Res.*, **1975**, *9*, 26-33. b) Sedó, S.; Ventosa, N.; Molins, M.A.; Pons, M.; Rovira, C.; Veciana, J. Stereoisomerism of molecular multipropellers. 1. Static stereochemistry of bis- and tris-triaryl systems. *J. Org. Chem.*, **2001**, *66*, 1567-1578. c) Wolf, C. *Dynamic stereochemistry of chiral compounds: Principles and applications*, The Royal Society of Chemistry, Cambridge CB4 0WF, UK, 2008

3 a) Kay, E.R.; Leigh, D.A.; Zerbetto, F. Synthetic molecular motors and mechanical machines. Angew. Chem. Int. Ed., 2007, 46, 72-191. b) Hanozin, E.; Mignolet, B.; Morsa, D.; Sluysmans, D.; Duwez, A.-S.; Stoddart, J.F.; Remacle, F.; De Pauw, E. Where ion mobility and molecular dynamics meet to unravel the (un)folding mechanisms of an oligorotaxane molecular switch. ACS Nano, 2017, 11, 10253-10263. c) Chen, Q.; Sun, J.; Li, P.; Hod, I.; Moghadam, P.Z.; Kean, Z.S.; Snurr, R.Q.; Hupp, J.T.; Farha, O.K.; Stoddart, J.F. A redox-active bistable molecular switch mounted inside a metal-organic framework. J. Am. Chem. Soc. 2016, 138, 14242-14245. d) Sun, J.; Wu, Y.; Wang, Y.; Liu, Z.; Cheng, C.; Hartlieb, K.J.; Wasielewski, M.R.; Stoddart, J.F. An electrochromic tristable molecular switch. J. Am. Chem. Soc. 2015, 137, 13484-13487. e) Sun, J.; Wu, Y.; Liu, Z.; Cao, D.; Wang, Y.; Cheng, C.; Chen, D.; Wasielewski, M.R.; Stoddart, J.F. Visible light-driven artificial molecular switch actuated by radical-radical and donor-acceptor interactions. J. Phys. Chem. A 2015, 119, 6317-6325. f) Grunder, S.; McGrier, P.L.; Whalley, A.C.; Boyle, M.M.; Stern, C.; Stoddart, J.F. A Water-soluble pHtriggered molecular switch. J.Am. Chem. Soc. 2013, 135, 17691-17694. g) Durola, F.; Heitz, V.; Reviriego, F.; Roche, C.; Sauvage, J.-P. Sour, A.; Trolez, S. Cyclic [4]rotaxanes containing two parallel porphyrinic plates: Toward switchable molecular receptors and compressors. Acc. Chem. Res. 2014, 47, 633-645.

4 a) Koumura, N.; Zijlstra, R.W.J.; van Delden, R.R.; Harada, N.; Feringa, B.L. Light-driven monodirectional molecular rotor. *Nature*, **1999**, *401*, 152-155. b) Faulkner, A.; van Leeuwen, T.; Feringa, B.L.; Wezenberg, S.J. allosteric regulation of the rotational speed in a light-driven molecular motor. *J. Am. Chem. Soc.* **2016**, *138*, 13597-13603. c) Collins, B.S.L.; Kistemaker, J.C.M.; Otten, E.; Feringa, B.L. A chemically powered unidirectional rotary molecular motor based on a palladium redox cycle. *Nat. Chem.* **2016**, *8*, 860-866. d) Vachon, J.; Carroll, G.T.;

Pollard, M.M.; Mes, E.M.; Brouwer, A.M.; Feringa, B.L. An ultrafast surface-bound photo-active molecular motor. *Photochem. Photobiol. Sci.* **2014**, *13*, 241-246. e) Ruangsupapichat, N.; Pollard, M.M.; Harutyunyan, S.R.; Feringa, B.L. Reversing the direction in a light-driven rotary molecular motor. *Nat. Chem.* **2010**, *3*, 53-60.

- 5 a) Cheng, C.; McGonigal, P. R.; Schneebeli, S. T.; Li, H.; Vermeulen, N. A.; Ke, C.; Stoddart, J. F. An artificial molecular pump, *Nature Nanotech.* **2015**, 10, 547-553. b) Pezzato, C.; Nguyen, M.T.; Cheng, C.; Kim, D.J.; Otley, M.T.; Stoddart, J.F. An efficient artificial molecular pump. *Tetrahedron* **2017**, *73*, 4849-4857.
- 6 a) Jiménez, M. C.; Dietrich-Buchecker, C.; Sauvage, J.-P. Towards synthetic molecular muscles: Contraction and stretching of a linear rotaxane dimer. *Angew. Chem., Int. Ed.* **2000**, 39, 3284. b) Niess, F.; Duplan, V.; Sauvage, J.-P. Molecular Muscles: From Species in Solution to Materials and Devices. *Chem. Lett.* **2014**, *43*, 964-974.
- 7 a) Zhanga, L.; Marcos, V.; Leigh, D. A. Molecular machines with bio-inspired mechanisms. *Proc. Nat. Acad. Sci.* 2018, *115*, 9397-9404. b) Erbas-Cakmak, S.; Leigh, D.A.; McTernan, C.T.; Nussbaumer, A.L. Artificial Molecular Machines. *Chem. Rev.*, 2015, *115*, 10081-10206. c) Ashton, P.R.; Balzani, V.; Kocian, O.; Prodi, L.; Spencer, N.; Stoddart, J.F. A Light-Fueled "Piston Cylinder" Molecular-Level Machine. *J. Am. Chem. Soc.*, 1998, *120*, 11190-11191. d) Le Poul, N.; Colasson, B. Electrochemically and Chemically Induced Redox Processes in Molecular Machines. *ChemElectroChem* 2015, *2*, 475-496. e) Baroncini, M.; Canton, M.; Casimiro, L.; Corra, S.; Groppi, J.; La Rosa, M.; Silvi, S.; Credi, A. Photoactive Molecular-Based Devices, Machines, and Materials: Recent Advances. *Eur. J. Inorg. Chem.* 2018, 4589-4603. f) Michl. J.; Sykes, C.H. Molecular Rotors and Motors: Recent Advances and Future Challenges. *ACS Nano* 2009, *3*, 1042-1048.

8 a) Badjić, J.D.; Balzani, V.; Credi, A.; Silvi, S.; Stoddart, J.F. A Molecular Elevator. *Science*, **2004**, *303*, 1845-1849. b) Kudernac, T.; Ruangsupapichat, N.; Parschau, M.; Maciá, B.; Katsonis, N.; Harutyunyan, S.R.; Ernst, K.-H.; Feringa, B.L. Electrically driven directional motion of a four-wheeled molecule on a metal surface. *Nature*, **2011**, *479*, 208-211.

- 9 a) Klichko, Y.; Liong, M.; Choi, E.; Angelos, S.; Nel, A.E.; Stoddart, J.F.; Tamanoi. F.; Zink, J.I. Mesostructured Silica for Optical Functionality, Nanomachines, and Drug Delivery. *J. Am. Ceram. Soc.*, **2009**, *92*, S2-S10. b) Ferris, D. P.; Zhao, Y.-L.; Khashab, N. M.; Khatib, H. A.; Stoddart, J. F.; Zink, J. I. Light-Operated Mechanized Nanoparticles, *J. Am. Chem. Soc.*, **2009**, *131*, 1686. c) Tarn, D.; Ashley, C.E.; Xue, M; Carnes, E.C.; Zink, J.I.; Brinker, C.J. Mesoporous Silica Nanoparticle Nanocarriers: Biofunctionality and Biocompatibility *Acc. Chem. Res.*, **2013**, *46*, 792-801
- 10 a) Mariani, G.; Goujon, A.; Moulin, E.; Rawiso, M.; Giuseppone, N.; Buhler, E. Integration of molecular machines into supramolecular materials: actuation between equilibrium polymers and crystal-like gels. *Nanoscale*, **2017**, *9*, 18456–18466; b) Asshoff, S.J.; Lancia, F.; Iamsaard, S.; Matt, B.; Kudernac, T.; Fletcher, S.P.; Katsonis, N. High-power actuation from molecular photoswitches in enantiomerically paired soft springs. *Angew. Chem. Int. Ed.*, 2017, 56, 3261-3265. c) Kwon, H.J.; Shikinaka, K.; Kakugo, A.; Gong, J.P.; Osada, Y. Gel biomachine based on muscle proteins. *Polymer Bulletin*, **2007**, *58*, 43-52.
- 11 a) Vogelsberg, C.S.; Garcia-Garibay, M.A. Crystalline molecular machines: function, phase order, dimensionality, and composition. *Chem. Soc. Rev.*, **2012**, *41*, 1892-1910. b) Khuong, T.V.; Nuñez, J.E.; Godinez, C.E.; Garcia-Garibay, M.A. Crystalline Molecular Machines: A Quest Toward Solid-State Dynamics and Function. *Acc. Chem. Res.* **2006**, *39*, 413-422. c) Garcia-

Garibay, M. A. Crystalline molecular machines: Encoding supramolecular dynamics into molecular structure. *Proc. Natl. Acad. Sci. U.S.A.* **2005**, *102*, 10771-10776.

12 Nargarkar, S.S.; Desai, A.V.; Ghosh, S.K. Stimulus-Responsive Metal-Organic Frameworks. *Chem. Asian J.* **2014**, *9*, 2358-2376.

13 a) Ellis, E.; Moorthy, S.; Chio, W.K.; Lee, T.-C. Artificial molecular and nanostructures for advanced nanomachinery. *Chem. Commun.* **2018**, *54*, 4075-4090. b) Abendroth, J.M.; Bushuyev, O.S.; Weiss, P.S.; Barrett, C.J. Controlling Motion at the Nanoscale: Rise of the Molecular Machines. *ACS Nano*, **2015**, *9*, 7746-7768. c) Endo, M.; Sugiyama, H. DNA Origami Nanomachines. *Molecules*, **2018**, *23*, 1766 d) Ariga, K.; Ito, H.; Hill, J.P.; Tsukube, H. Molecular recognition: from solution science to nano/materials technology. *Chem. Soc. Rev.*, **2012**, *41*, 5800-5835.

14 a) Naumov, P.; Chizhik, S.; Panda, M. K.; Nath, N. K.; Boldyreva, E. Mechanically responsive molecular crystals. *Chem. Rev.* 2015, *115*, 12440–12490. b) Takanabe, A.; Tanaka, M.; Johmoto, K.; Uekusa, H.; Mori, T.; Koshima, H.; Asahi, T. Optical activity and optical anisotropy in photomechanical crystals of chiral salicylidenephenylethylamines. *J. Am. Chem. Soc.* 2016, *138*, 15066–15077. c) Kim, T.; Al-Muhanna, M. K.; Al-Suwaidan, S. D.; Al-Kaysi, R. O.; Bardeen, C. J. Photoinduced Curling of Organic Molecular Crystal Nanowires. *Angew. Chem. Int. Ed.* 2013, *52*, 6889–6893. d) Kitagawa, D.; Tsujioka, H.; Tong, F.; Dong, X.; Bardeen, C. J.; Kobatake, S. Control of Photomechanical Crystal Twisting by Illumination Direction. *J. Am. Chem. Soc.* 2018, *140*, 4208–4212.

15 Viswanathan, B. *Structure and Properties of Solid State Materials*; Alpha Science Intl. Ltd.: Oxford, UK, 2006.

16 a) Kushida, S.; Smarsly, E.; Bojanowski, N.M.; Wacker, I.; Schröder, R.R.; Oki, O.; Yamamoto, Y.; Melzer, C.; Bunz, U.H.F. Dipole-Switchable Poly(para-phenyleneethynylene)s: Ferroelectric Conjugated Polymers. Angew. Chem. Int. Ed., 2018, 57, 17019-17022. b) Kaleta, J.; Wen, J.; Magnera, T.F.; Dron, P.I.; Zhu, C.; Michl, J. Structure of a monolayer of molecular rotors on aqueous subphase from grazing-incidence X-ray diffraction. Proc. Nat. Acad. Sci. USA, 2018, 115, 9373-9378. c) Dron, P.I.; Zhao, K.; Kaleta, J.; Shen, Y.; Wen, J.; Shoemaker, R.K.; Rogers, C.T.; Michl, J. Bulk Inclusions of Pyridazine-Based Molecular Rotors in Tris(ophenylenedioxy)cyclotriphosphazene (TPP). Adv, Funct. Mater., 2016, 26, 5718-5732. d) Horinek, D.; Michl, J. Molecular dynamics of a grid-mounted molecular dipolar rotor in a rotating electric field. Proc. Nat. Acad. Sci. USA, 2005, 102: 14175-14180. e) Vacek, J.; Michl. J. Artificial Surface-Mounted Molecular Rotors: Molecular Dynamics Simulations, Adv. Funct. Mater. 2007, 17, 730–739. f) Thomas, J.C.; Schwartz, J.J.; Hohman, J.N.; Claridge, S.A.; Auluck, H.S.; Serino, A.C.; Spokoyny, A.M.; Tran, G.; Kelly, F.; Mirkin C.A.; Gilles, J.; Osher, S.J.; Weiss, P.S. Defect tolerant aligned dipoles within two-dimensional lattices. ACS Nano, **2015**, 9, 4734-4742.

17 Kottas, G.S.; Clarke, L.I.; Horinek, D.; Michl, J. Artificial Molecular Rotors. *Chem. Rev.* **2005**, *105*: 1281-1376.

18 a) Rozenbaum, V. M. Orientation states of dipoles on 2D Bravais lattices. *Sov. Phys. JETP* **1991**, *72*, 1028. b) Rozenbaum, V. M. Ground state and vibrations of dipoles on a honeycomb lattice. *Phys. Rev. B* **1995**, *51*, 1290. c) Rozenbaum, V. M. Coulomb interactions in two-dimensional lattice structures. *Phys. Rev. B* **1996**, *53*, 6240. d) Rozenbaum, V. M. Long-range orientational order in a two-dimensional degenerate system of dipoles on a square lattice *JETP Lett.*, **1996**, *63*, 662-667.

- 19 Karlen, S.D.; Garcia-Garibay, M.A. Amphidynamic crystals: Structural blueprints for molecular machines. *Top. Curr. Chem.*, **2005**, *262*, 179-227.
- 20 Gould, S.L.; Tranchemontagne, D.; Yaghi, O.M.; Garcia-Garibay, M.A. Amphidynamic Character of Crystalline MOF-5: Rotational Dynamics of Terephthalate Phenylenes in a Free-Volume, Sterically Unhindered Environment. *J. Am. Chem. Soc.* **2008**, *130*, 3246-3247.
- 21 Vogelsberg, C.S.; Uribe-Romo, F.J.; Lipton, A.S.; Yang, S.; Houk, K.N.; Brown, S.; Garcia-Garibay, M.A. Ultrafast rotation in an amphidynamic crystalline metal organic framework. *Proc. Natl. Acad. Sci.*, **2017**, *114*, 13613-13618.
- 22 Zhu, K.; O'Keefe, C.A.; Vukotic, N.; Schurko, R.W.; Loeb, S.J. A molecular shuttle that operates inside a metal-organic framework. *Nature Chemistry*, **2015**, *7*, 514-519.
- 23 a) Inukai, M.; Tamura, M.; Horike, S.; Higuchi, M.; Kitagawa, S.; Nakamura, K. Storage of CO₂ into Porous Coordination Polymer Controlled by Molecular Rotor Dynamics. *Angew. Chem. Int. Ed.*, **2018**, *57*, 8687-8690. b) Gu, C.; Hosono, N.; Zheng, J.-J.; Kusaka, S.; Sakaki, S.; Kitagawa, S. Design and control of gas diffusion process in a nanoporous soft crystal. *Science*, **2019**, *363*, 387-391.
- 24 Karlen, S.D.; Reyes, H.; Taylor, R.E.; Khan, S.I.; Hawthorne, F.; Garcia-Garibay, M.A. Symmetry and dynamics of molecular rotors in amphidynamic molecular crystals. *Proc. Natl. Acad. Sci.* **2010**, 14973-14977.
- 25 Jiang, X.; Rodriguez-Molina, B.; Nazarian, N.; Garcia-Garibay, M.A. Rotation of a Bulky Triptycene in the Solid State: Towards Engineered Nanoscale Artificial Molecular Machines. *J. Am. Chem. Soc.* **2014**, *136*, 8871–8874.
- 26 a) Beckmann, P. A., Schneider, E. Methyl group rotation, ¹H spin-lattice relaxation in an organic solid, and the analysis of nonexponential relaxation. *J. Chem. Phys.* **2012**, *136*, 054508.

b) Wang, X.; Beckmann, P. A.; Mallory, C. W.; Rheingold, A. L.; DiPasquale, A. G.; Carroll, P. J.; Mallory, F. B., Intramolecular and intermolecular contributions to the barriers for rotation of methyl groups in crystalline solids: Electronic structure calculations and solid-state NMR relaxation measurements. *J. Org. Chem.* 2011, 76, 5170. c) Conn, K. G.; Beckmann, P. A.; Mallory, C. W.; Mallory, F. B. Methyl reorientation in methylphenanthrenes. I. Solid state proton spin-lattice relaxation in the 3-methyl, 9-methyl, and 3,9-dimethyl systems *J. Chem. Phys.* 1987, 87, 20-27. d) Wang, X.; Rotkina, L.; Su, H.; Beckmann, P. A. Single-crystal x-ray diffraction, isolated molecule and cluster electronic structure calculations, and scanning electron microscopy in an organic solid: models for intramolecular motion in 4,4' dimethoxybiphenyl. *Chem. Phys. Chem.* 2012, 13, 2082-2089.

27 a) Lemouchi, C.; Vogelsberg, C.S.; Zorina, L.; Simonov, S.; Batail, P.; Brown, S.; Garcia-Garibay, M.A. Ultra-fast rotors for molecular machines and functional materials via halogen bonding: crystals of 1,4-bis(iodoethynyl)bicyclo[2.2.2]octane with distinct gigahertz rotation at two sites. *J. Am. Chem. Soc.*, **2011**, *133*, 6371-6379. b) Lemouchi, C.; Mézière, C.; Zorina, L.; Simonov, S.; Rodríguez-Fortea, A.; Canadell, E.; Wzietek, P.; Auban-Senzier, P.; Pasquier, C.; Giamarchi, T; Garcia-Garibay, M.A.; Batail, P. Design and evaluation of a crystalline hybrid of molecular conductors and molecular rotors. *J. Am. Chem. Soc.*, **2012**, *134*, 7880-7891. c) Rodríguez-Molina, B.; Pérez-Estrada, S.; Garcia-Garibay, M.A. Amphidynamic crystals of a steroidal bicyclo[2.2.2]octane rotor: a high symmetry group that rotates faster than smaller methyl and methoxy groups. *J. Am. Chem. Soc.*, **2013**, *135*, 10388-10395.

28 Hill, J.G.; Platts, J.A.; Werner, H.-J. Calculation of intermolecular interactions in the benzene dimer using coupled-cluster and local electron correlation methods. *Phys. Chem. Chem. Phys.*, **2006**, *8*, 4072–4078.

- 29 Yaghi, O.; Li, H.; Davis, C.; Richardson, D.; Groy, T.L. Synthetic strategies, structure patterns, and emerging properties in the chemistry of modular porous solids. *Acc. Chem. Res.*, **1998**, *31*, 474-484.
 - 30 Kitaigorodsky, A. I. Molecular crystals and molecules, Academic Press, New York, 1973.
- 31 Hiroyasu Furukawa, H.; Ko, N.: Go, Y.B.; Aratani, N.; Choi, S.B.; Choi, E.; Yazaydin, A. Ö.; Snurr, R. Q.; O'Keeffe. M.; Kim, J.:Yaghi, O., Ultrahigh porosity in metal-organic frameworks, *Science*, **2010**, 329, 424-428.
 - 32 Spartan'08 Wavefunction, Inc. Irvine, CA.
- 33 (a) Gavezzotti, A. The calculation of molecular volumes and the use of volume analysis in the investigation of structured media and of solid-state organic reactivity. *J. Am. Chem. Soc.* **1982**, *105*, 5220–5225. (b) Bondi, A. van der Waals volumes and radii. *J. Phys. Chem.* **1964**, *68*, 441-451.
- 34 Eddaoudi, M.; Kim, J.; Rosi, N.; Vodak, D.; Wachter, J.; O'Keeffe, M.; Yaghi, O.M. Systematic Design of Pore Size and Functionality in Isoreticular MOFs and Their Application in Methane Storage. *Science*, **2002**, *295*, 469-472.
- 35 Winston, E.B.; Lowell, P.J.; Vacek, J.; Chocholoušová, J.; Michl, J.; Price, J.C. Dipolar molecular rotors in the metal-organic framework crystal IRMOF-2 *Phys. Chem. Chem. Phys.* **2008**, *10*, 5188-5191.
- 36 Morris, W.; Taylor, R.E.; Dybowski, C.; Yaghi, O.M.; Garcia-Garibay, M.A. Framework mobility in the metal-organic framework crystal IRMOF-3: Evidence for aromatic ring and amine rotation. *J. Mol. Struct.* **2011**, *1004*, 94-101.
- 37 Rotation about alkynyl single bonds is nearly frictionless: (a) Saebo, S.; Almlöf, J.; Boggs, J. E.; Stark, J. G. Two approaches to the computational determination of molecular structure: the

torsional angle in tolane and the effect of fluorination on the structure of oxirane. *J. Mol. Struct.* (*Theochem*) **1989**, 200, 361-373. (b) Sipachev, V. A.; Khaikin, L. S.; Grikina, O. E.; Nikitin, V. S.; Trættberg, M. Structure, spectra and internal rotation of bis(trimethylsilyl) acetylene: spectral analysis by scaling quantum-chemical force fields and two methods for calculating vibrational effects. *J. Mol. Struct.* **2000**, *523*, 1-22.

- 38 Jarowski, P.D.; Houk, K.N.; Garcia-Garibay, M.A. Importance of correlated motions on the low barrier rotational potentials of crystalline molecular gyroscopes. *J. Am. Chem. Soc.*, **2007**, *129*, 3110-3117.
- 39 Minamino T.; Imada, K.; Namba, K. Molecular motors of the bacterial flagella, *Curr. Opin. Struct. Biol.*, **2008**,18, 693-701.
- 40 Akutagawa, T.; Koshinaka, H.; Sato, D.; Takeda, S.; Noro, S.I.; Takahashi, H.; Kumai, R.; Tokura, Y.; Nakamura, T. Ferroelectricity and polarity control in solid state flip-flop supramolecular rotors, *Nature Materials* **2009**, *8*, 342-347.
- 41 Vacek, J.; Michl, J. Molecular dynamics of a grid-mounted molecular dipolar rotor in a rotating electric field, *Proc. Nat. Acad. Sci. USA* **2001**, *98*, 5481-5486.
- 42 As compared to BCO, *para*-carborane rotators belong in the point group S_n and have an inversion center (*i*), such that rotational disorder does not generate a higher symmetry space group.
- 43 a) Catalano, L.; Perez-Estrada, S.; Wang, H.-H.; Ayitou, A. J.-L.; Khan, S.I.; Terraneo, G.; Metrangolo, P.; Brown, S.; Garcia-Garibay, M.A. Rotational dynamics of diazabicyclo[2.2.2]octane in isomorphous halogen-bonded co-crystals: entropic and enthalpic effects. *J. Am. Chem. Soc.*, **2017**, *139*, 843-848. b) Karlen, S.D.; Ortiz, R.; Chapman, O.L.;

Garcia-Garibay, M.A. Effects of rotational symmetry order on the solid state dynamics of phenylene and diamantane rotators. *J. Am. Chem. Soc.*, **2005**, *127*, 6554-6555.

44 Catalano, L.; Pérez-Estrada, S.; Terraneo, G.; Pilati, T.; Resnati, G.; Metrangolo, P.; Garcia-Garibay, M.A. Dynamic characterization of crystalline supramolecular rotors assembled through halogen bonding. *J. Am. Chem. Soc.*, **2015**, *137*, 15386-15389.

45 Godinez, C.E.; Zepeda, G.; Garcia-Garibay, M.A. Molecular compasses and gyroscopes. ii. synthesis and characterization of molecular rotors and axially substituted bis[2-(9-triptycyl)ethynyl]arenes. *J. Am. Chem. Soc.*, **2002**, *124*, 4701-4707.

46 Dominguez, Z.; Dang, H.; Strouse, M.J.; Garcia-Garibay, M.A. Molecular "compasses" and "gyroscopes." I. Expedient synthesis and solid state dynamics of an open rotor with a bis(triarylmethyl) frame. *J. Am. Chem. Soc.*, **2002**, *124*, 2398-2399.

47 Dominguez, Z.; Dang, H.; Strouse, M.J.; Garcia-Garibay, M.A. Molecular "compasses" and "gyroscopes." III. Dynamics of a phenylene rotor and clathrated benzene in a slipping-gear crystal lattice. *J. Am. Chem. Soc.*, **2002**, *124*, 7719-7727.

48 a) Horansky, R.D.; Clarke, L.I.; Price, J.C.; Khuong, T.-A.V.; Jarowski, P.D.; Garcia-Garibay, M.A. Dielectric response of a dipolar molecular rotor crystal. *Phys. Rev. B.*, **2005**, *72*, 014302. b) Horansky, R.D.; Clarke, L.I.; Winston, E.B.; Price, J.C.; Karlen, S.D.; Jarowski, P.D.; Santillan, R.; Garcia-Garibay, M.A. Dipolar rotor-rotor interactions in a difluorobenzene molecular rotor crystal. *Phys. Rev. B*, **2006**, *74*, 054306. c) Rodriguez-Molina, B.; Ochoa, M.E.; Farfán, N.; Santillan, R.; Garcia-Garibay, M.A. Synthesis, characterization, and rotational dynamics of crystalline molecular compasses with n-heterocyclic rotators. *J. Org. Chem.*, **2009**, *74*, 8554-8565. d) Jin, M.; Chung, T.S.; Seki, T.; Ito, H.; Garcia-Garibay, M.A. Phosphorescence control mediated by molecular rotation and aurophilic interactions in amphidynamic crystals of

1,4-bis[tri-(*p*-fluorophenyl)phosphane-gold(I)-ethynyl]benzene. *J. Am. Chem. Soc.*, **2017**, *139*, 18115-18121. e) Commins, P.; Garcia-Garibay, M.A. Photochromic Molecular Gyroscope with Solid State Rotational States Determined by an Azobenzene Bridge. *J. Org. Chem.*, **2014**, *79*, 1611-1619. f) Karlen, S.D.; Godinez, C.E.; Garcia-Garibay, M.A. Improved Physical Properties and Rotational Dynamics in a Molecular Gyroscope with an Asymmetric Stator Structure. *Org. Lett.*, **2006**, *8*, 3417-3420. g) Staehle, I.O.; Rodríguez-Molina, B.; Khan, S.I.; Garcia-Garibay, M.A. Engineered Photochromism in Crystalline Salicylidene Anilines by Facilitating Rotation to Reach the Colored *trans*-Keto Form. *Cryst. Growth Des.*, **2014**, *14*, 3667-3673. h) Hughs, M.; Jimenez, M; Khan, S.; Garcia-Garibay, M.A. Synthesis, Rotational Dynamics, and Photophysical Characterization of a Crystalline Linearly Conjugated Phenyleneethynylene Molecular Dirotor. *J. Org. Chem.*, **2013**, *78*, 5293-5302.

49 Garcia-Garibay, M.A.; Godinez, C.E. Engineering crystal packing and internal dynamics in molecular gyroscopes by refining their components. fast exchange of a phenylene rotator by ²H NMR. *Cryst. Growth Des.*, **2009**, *9*, 3124-3128.

50 a) Khuong, T.-A.V.; Zepeda, G.; Ruiz, R.; Khan, S.I.; Garcia-Garibay, M.A. Molecular compasses and gyroscopes: engineering molecular crystals with fast internal rotation. *Crystal Growth & Design*, **2004**, *4*, 15-18. b) Khuong, T.-A.V.; Dang, H.; Jarowski, P.D.; Maverick, E.F.; Garcia-Garibay, M.A. Rotational dynamics in a crystalline molecular gyroscope by variable-temperature ¹³C NMR, ²H NMR, X-ray diffraction, and force field calculations. *J. Am. Chem. Soc.*, **2007**, *129*, 839-845. c) O'Brien, Z.J.; Natarajan, A.; Khan, S.; Garcia-Garibay, M.A. Synthesis and solid-state rotational dynamics of molecular gyroscopes with a robust and low density structure built with a phenylene rotator and a tri(*meta*-terphenyl)methyl stator. *Cryst. Growth Des.*, **2011**, *11*, 2654-2659. d) Arcos-Ramos, R.; Rodriguez-Molina, B; Gonzalez-

Rodriguez, E.; Ramirez-Montes, P.I.; Ochoa, M.E.; Santillan, R.; Farfán, N.; Garcia-Garibay, M.A. Crystalline arrays of molecular rotors with TIPS-trityl and phenolic-trityl stators using phenylene, 1,2-difluorophenylene and pyridine rotators. *RSC Adv.*, **2015**, *5*, 55201-55208.

51 Jiang, X.; O'Brien, Z.J.; Yang, S.; Lai, L.H.; Buenaflor, J.; Tan, C.; Khan, S.; Houk, K.N.; Garcia-Garibay, M.A. Crystal fluidity reflected by fast rotational motion at the core, branches, and peripheral aromatic groups of a dendrimeric molecular rotor. *J. Am. Chem. Soc.*, **2016**, *138*, 4650-4656.

52 Kawski, A. Fluorescence anisotropy: theory and applications of rotational depolarization. *Critical Reviews in Analytical Chemistry*, **1993**, *23*, 459-529.

53 Vogelsberg, C.S.; Bracco, S.; Beretta, M.; Comotti, A.; Sozzani, P.; Garcia-Garibay, M.A. Dynamics of molecular rotors confined in two dimensions: transition from a 2d rotational glass to a 2D rotational fluid in a periodic mesoporous organosilica. *J. Phys. Chem. B*, **2012**, *116*, 1623-1632.

54 a) Lorbach, A.; Maverick, E.; Carreras, A.; Alemany, Pere; Wu, Gang,; Garcia-Garibay M.A; Bazan, G.C. "A Fullerene–carbene adduct as a crystalline molecular rotor: remarkable behavior of a spherically-shaped rotator." *Phys. Chem. Chem. Phys.*, **2014**, *16*, 12980-12986; b) Pekker, S.; Kovats, E.; Oszlanyi, G.; Benyei, G.; Klupp, G.; Bortel, G.; Jalsovszky, I.; E. Borondics, J.F.; Karnaras, K.; Bokor, M.; Kriza, G.; Tompa, K.; Faigel, G. Rotor-stator molecular crystals of fullerenes and cubane, *Nature Materials*, 2005, **4**, 764-767.

55 a) Ye, H.Y.; Li, S.H.; Zhang, Y.; Zhou, L.; Deng, F.; Xiong, R.-G. Solid state molecular dynamic investigation of an inclusion ferroelectric: [(2.6-diisopropylanilinium)[18]crown-6)]BF₄, *J. Am. Chem. Soc.* **2014**, *136*, 10033-10044. b) Harada, J.; Shimojo, T.; Oyamaguchi, H.; Hasegawa, H.; Takahashi, Y.; Satomi, K.; Suzuki, Y.; Kawamata, J.; Inabe, T. Directionally

tunable and mechanically deformable ferroelectric crystals from rotating polar globular ionic molecules, *Nature Chem.* **2016**, *8*, 946-952. c) Akutagawa, T.; Koshinaka, H.; Sato, D.; Takeda, S.; Noro, S.-I.; Takahashi, H.; Kumai, R.; Tokura, Y.; Nakamura, T. Ferroelectric and polarity control in solid-state flip-flop supramolecular rotors, *Nat. Mater.* **2009**, *8*, 342-347. d) Zhang, W.; Xiong, R.-G.; Yoshikawa, H.; Awaga, K. Exceptional dielectric phase transition in a pervoskite-type cage compound, *Angew. Chem. Int. Ed.* **2010**, *49*, 6608-6610. e) Sun, Z.; Chen, T.; Luo, J.; Hong, M. Bis(imidazolium) L-tartrate: A hydrogen bonded displacive molecular ferroelectric material, *Angew. Chem. Int. Ed.* **2012**, *51*, 3871-3876.

Table of Contents Graphic

